5

Space Coordinate Transformation and Applications

André de Lustrac, Shah Nawaz Burokur, Paul-Henri Tichit, Boubacar Kante, Rasta Ghasemi and Dylan Germain
Institut d'Electronique Fondamentale, Univ. Paris-Sud, CNRS UMR 8622, Orsay, France

1. Introduction

Invisibility or cloaking is an old myth of humanity that must date probably from the time when the success in hunting or war would depend on the ability to hide as much as possible. This invisibility, after being a prolific subject for writers and filmmakers, has become almost a reality in 2006 with the first practical realization of an electromagnetic invisibility cloak.

The invariance of Maxwell's equations in the geometric transformation of coordinates has become a hot topic that year with the first proposal of a cylindrical invisibility cloak by J. B. Pendry and U. Leonhardt. The experimental fabrication and characterization of the first cloak at microwave frequencies have shown that this tool is very effective. After this realization, several applications of this transformation have been proposed for the design of concentrators, waveguides, transitions and bends, directional antennas, and even electromagnetic wormholes.

This space transformation is therefore a powerful tool for the design of devices or components with special properties difficult to obtain from conventional materials and geometries. Theoretically, the method of coordinate transformation involves the generation of a new space derived from an original space where the solutions of Maxwell's equations are known.

The first step is to imagine an initial space and a final space with their topological properties and link them through an analytic transformation. Most of this work is based on a continuous transformation that produces a final space with electromagnetic parameters often complex, heterogeneous and anisotropic.

The challenge is then to effectively design this new space. To make the fabrication easier, simplified parameters were proposed in the early works, with the disadvantage of an impedance mismatch between the material and its environment. More recently, a transformation applied to discrete multi-layer structures has been proposed to further simplify the realization. In this chapter, we present the principles and main applications envisaged for this transformation.

2. Space coordinate transformation

2.1 Principle

In a letter of 1662 Pierre de Fermat established the principle that governs the geometrical optics [Tannery, 1891]. The light follows a stationary optical path between two points. Most of the time, it follows the shortest path. In some cases, it takes the longer one. The optical path is defined by the equation 1, where n is the refractive index of the space, which may depend on the spatial coordinates, and dl a small element of distance:

$$s = \int ndl \tag{1}$$

If n varies with the position in space the path followed by the light can be bent instead of following a straight line. This occurs, for example over a hot road in summer when the index of the air layers above the road varies with the temperature and the height over the road. In this case we can observe a curvature of the path followed by the sunlight that gives the impression that the road is covered with water. Figure 1 shows a schematic of the path of light when the space is not distorted and when this space is distorted (Figure 1a and b).

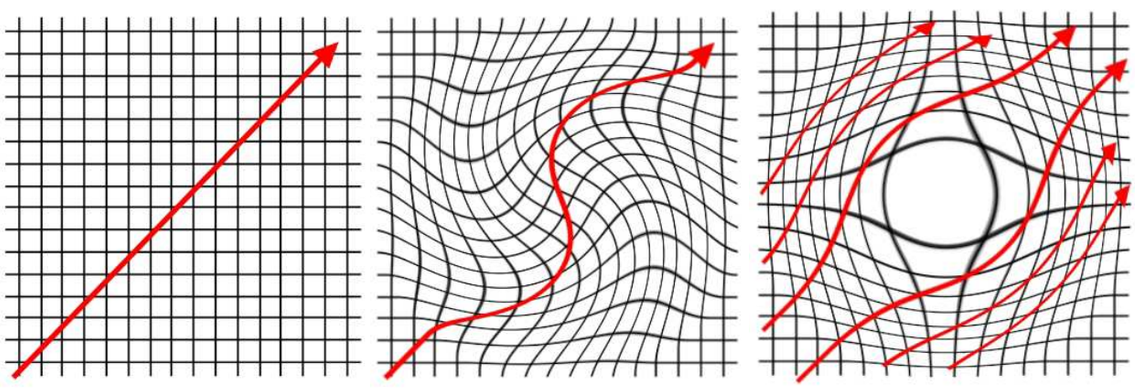

(a) (b) (c)

Fig. 1. (a) Propagation of a light beam in a non distorted space. (b) propagation of the same ray of light in a distorted space. (c) isolation of a region of space by deforming the propagation of light rays around this region.

J. Pendry and U. Leonhardt noted both in their articles published in 2006, the invariance of Maxwell's equations in such a deformed space [Pendry, 2006, Leonhardt, 2006]. J. Pendry has concluded that it was possible to isolate a zone of space by bending light rays around this area (Figure 1c).

2.2 Implementation

The implementation of this transformation is relatively simple. If we consider a Cartesian space where each point is identified by three coordinates (x, y, z), we can define a new space where each point will be identified by three new coordinates (u, v, w). These three new coordinates are based on the original ones.

$$u(x,y,z), v(x,y,z), \text{ and } w(x,y,z) \tag{2}$$

In this case, we use normalized values of the electromagnetic parameters ε and μ that we will define in the new space:

$$\varepsilon'_u = \varepsilon_u \frac{F_u F_v F_w}{F_u^2} \text{ and } \mu'_u = \mu_u \frac{F_u F_v F_w}{F_u^2} \text{ ; etc…} \tag{3}$$

where F_u, F_v et F_w are defined by the following equations:

$$F_u = \left(\frac{\partial x}{\partial u}\right)^2 + \left(\frac{\partial y}{\partial u}\right)^2 + \left(\frac{\partial z}{\partial u}\right)^2 \quad F_v = \left(\frac{\partial x}{\partial v}\right)^2 + \left(\frac{\partial y}{\partial v}\right)^2 + \left(\frac{\partial z}{\partial v}\right)^2$$
$$\text{and } F_w = \left(\frac{\partial x}{\partial w}\right)^2 + \left(\frac{\partial y}{\partial w}\right)^2 + \left(\frac{\partial z}{\partial w}\right)^2 \tag{4}$$

The conventionnal relations of electromagnetics are conserved in the new space :

$$\vec{B}' = \mu_0 \mu' \vec{H}' \quad \text{and} \quad \vec{E} = \varepsilon_0 \varepsilon' \vec{E}' \tag{5}$$

In these relations, μ' and ε' are tensors whose components depend on the spatial coordinates u, v et w. Generally, the new space is anisotropic.

3. Cloaking

The first application of the space coordinate transformation will be the design and the characterization of different electromagnetic invisibility cloaks [2-6].

3.1 Principle

In the case of the first invisibility cloak proposed by Smith and Pendry [Pendry, 2006], the transformation of space concerned a cylindrical space of radius b which is transformed into an annular space between radii a and b (Figure 2). The initial points in space are identified by coordinates r, θ and z. Those of the transformed space are identified by r ', θ' and z' in cylindrical coordinates. Both spaces are assumed infinite in the directions z and z ', which are combined.

The transformation is defined by a relatively simple set of equations (6).

$$r' = \frac{b-a}{b} r + a \text{ ; } \theta' = \theta \text{ ; } z' = z \tag{6}$$

After transformation we obtain :

$$\varepsilon_r = \mu_r = \frac{r-a}{r} \text{ ; } \varepsilon_\theta = \mu_\theta = \frac{r}{r-a} \text{ ; } \varepsilon_z = \mu_z = \left(\frac{b}{b-a}\right)^2 \frac{r-a}{r} \tag{7}$$

The three parameters obtained depend on the distance r and on the geometric parameters of the original and transformed spaces. These are the electromagnetic parameters of the

transformed space. Note that the permeability and permittivity have here the same expressions. This guarantees the matching of the wave impedance of the transformed medium with the initial medium.

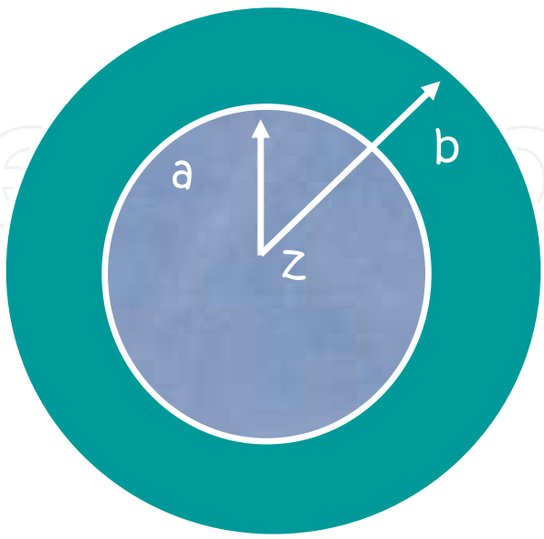

Fig. 2. Initial circular space of radius b, transformed to a ring between a and b.

3.2 Realization of the first microwave cloak

The practical realization of the material forming the transformed space is a difficult task since the three parameters vary simultaneously [Schurig, 2006]. To simplify this material, one solution is to choose a polarization, namely the transverse magnetic (TM) polarization, with the electric field E parallel to the axis z. In this case, only the parameters ε_z, μ_r et μ_θ are important. In this case, a simple set of parameters is possible provided it meets the propagation equation. The next set is one of the possibilities:

$$\varepsilon_z = \left(\frac{b}{b-a}\right)^2 ;\ \mu_r = \left(\frac{r-a}{r}\right)^2 ;\ \mu_\theta = 1 \tag{8}$$

In these three parameters, two are fixed and one varies; the radial permeability u_r. This material can be realized by the metamaterial concept [Soukoulis, 2011]. Figure 3a shows the basic pattern of the material and the geometric values used with the corresponding values of u_r. The permittivity ε_z is realized using a conventional dielectric.

Figure 3c shows a part of the realized circuit with, in the insert, the evolution of the three parameters μ_r, μ_θ and ε_z. The shape of the elementary patterns depends on the layer of material so that the permeability μ_r also varies and follows the red curve in the figure inset. Figure 4(a) and 4(b) shows the simulation of the cloak with respectively the theoretical parameters of equation 13 and the reduced parameters of equation 14. Figure 4(c) presents the measured electric field cartography of the central bare metallic cylinder where we can observe strong reflections and shadows compared to the case of very low reflections when the cloak is applied around the cylinder (Figure 4(d)).

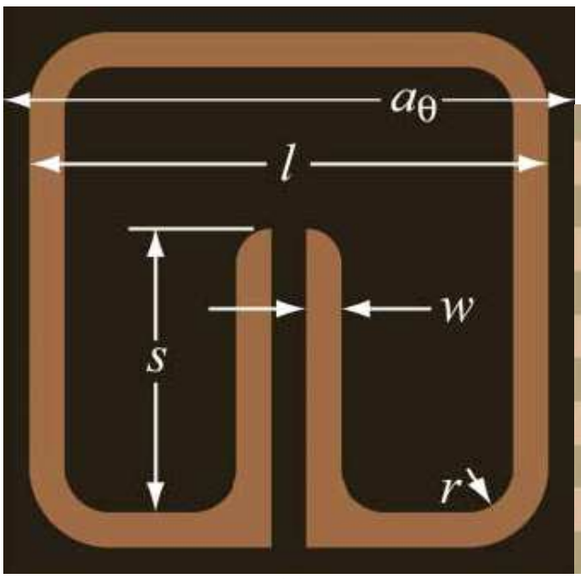

(a)

cyl.	r	s	μ_r
1	0.260	1.654	0.003
2	0.254	1.677	0.023
3	0.245	1.718	0.052
4	0.230	1.771	0.085
5	0.208	1.825	0.120
6	0.190	1.886	0.154
7	0.173	1.951	0.188
8	0.148	2.027	0.220
9	0.129	2.110	0.250
10	0.116	2.199	0.279

(b)

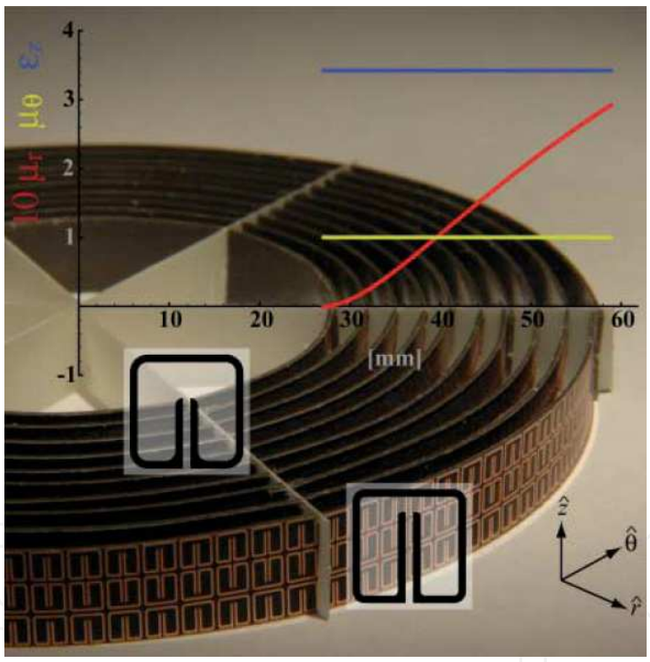

(c)

Fig. 3. (a) Elementary cell of the metamaterial. (b) values of the parameters. (c) Photography of the prototype. The insert shows the variations of μ_r, μ_θ and ε_z.

Figures 4b and 4d are quite similar and clearly show the influence of electromagnetic radiation on the cloak with in particular the cloaking of the central metallic cylinder by the electromagnetic energy. Both figures also illustrate the limits of the exercise as the use of a reduced set of parameters causes reflection of part of the incident energy, and therefore an imperfect reconstruction of the wave after the cloak.

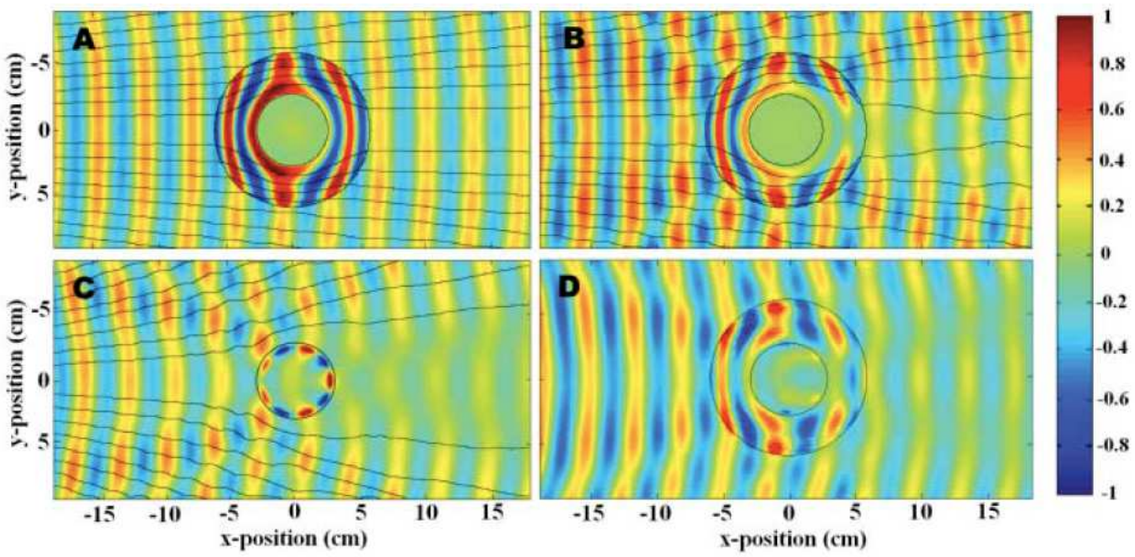

Fig. 4. (a) Simulation of the theoretical cloak. (b) simulation of the cloak with reduced parameters. (c) simulation of the central metallic cylinder. (d) E field measurement.

3.3 Others realizations

The experimental verification of this first cloak has excited the imagination of researchers who have tried to extend to other areas in optics but also in acoustics.

3.3.1 Cloak insensitive to the polarization

In the field of electromagnetics, few achievements have been proposed and tested experimentally. But there are some exceptions [Guven, 2008, Kante, 2008, Kante, 2009]. In reference [Guven, 2008], S. Tretyakov and his team tried to design a cloak based on spiral type resonators and the principle of homogenization. These coils act as a combination of an electric and a magnetic dipole. They can therefore meet the criteria to realize the material of the cloak. Fig. 5a shows the unit spiral resonator cell used by S. Tretyakov and Fig. 5b illustrates the distribution of the resonators in the cloak. The realization of the cloak is simpler than that of Smith and is supposed to work for both TM and TE polarizations of the incident wave with the disadvantage of its large size compared to the cloaked object.

3.3.2 Cloak based on the electric resonance of the SRR

In the references [Kante, 2008, Kante, 2009] the principle is completely different. Instead of using the magnetic resonance of the resonators of Pendry, the authors use the electrical resonance of these resonators. Smith's cloak works for a TM polarization (E-field vertical and H-field in the plane of the cloak). The new cloak works with a TE polarized wave (H-field vertical and E-field in the plane of the cape). For this non-magnetic cloak, the set of parameters is as follows:

$$\mu_z = 1\,,\quad \varepsilon_\theta = \left(\frac{b}{b-a}\right)^2,\quad \varepsilon_r = \left(\frac{b}{b-a}\right)^2\left(\frac{r-a}{r}\right)^2 \tag{9}$$

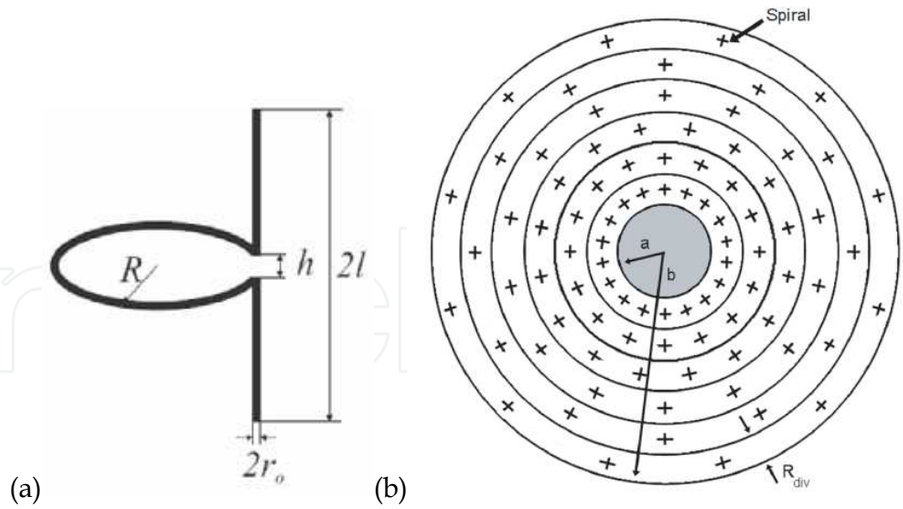

(a) (b)

Fig. 5. (a) Spiral coil used by S. Tretyakov in his cloak. (b) schematic view of the cloak.

This reduced set of parameters holds for a polarization perpendicular to the cylinder axis and satisfies the dispersion relation, but not the equality of the wave impedance between the vacuum and the cloak. A non-zero reflection is then predictable. In our implementation, the radial permittivity profile is designed using the electric response of SRRs by locally changing the dimension of resonators, actually only the SRRs gap size. The typical unit cell and the effective parameters of discrete SRRs at the design frequency (11 GHz) are presented in Fig. 6. While SRRs (embedded in the host medium) are used to achieve the radial variation of the permittivity function, the azimuthal permittivity is mainly implemented by the permittivity of the host medium itself since SRRs have no electric response in this direction. The realized cloak is composed of 15700 elementary SRRs. The cylindrical shell is divided in 20 annular regions of equal thickness (l_r=4.5 mm) with a linear radial variation of the permittivity from 0 to 1 (from the inner to the outer boundary of the cloak) and 157 stripes separated by an angle of about 2.3° (Fig.7 (a)). The inner and outer radius of the cloak are a=6 cm, b=15 cm and the cloak height is 2.25 cm corresponding to $5\times l_z$ i.e. 5 SRR layers. For this set of parameters the reflection coefficient R_p is very weak, equal to 0.0625. The SRRs within a given annular region are identical and designed to have the proper local radial permittivity. The host medium, a commercially available resin is an important design component (closely linked to ε_θ). Its permittivity has been measured and found to be equal to ε_{resin}= 2.75. The SRRs have been printed on a dielectric substrate (as seen in the picture of Fig.1 (c)) with a permittivity close to the resin's one. We chose RO3003 with $\varepsilon_{substrate}$= 3±0.04 and a dielectric loss tangent at 11 GHz of about 0.0013. The 157 stripes were arranged in a moulded water-tight polymeric matrix designed accordingly (Fig. 7 (a)).

In contrast with previously reported structure, the measurements are performed in free space and not in a waveguide configuration(Fig. 7b). A loop antenna, consisting of a circular coil made of the inner conductor of a SMA cable has been designed to map the magnetic field (H_z). The magnetic field is output from the X-band horn antenna. Both antennas are connected to an Agilent 8722ES Vectorial Network Analyzer. The loop antenna position can be controlled via an automated Labview program over a surface of 40 cm*40 cm and getting for each spatial position of the loop antenna the complex (magnitude and phase) scattering parameters. The experimental setup can be seen on Fig. 7(b). Since the resin fills the

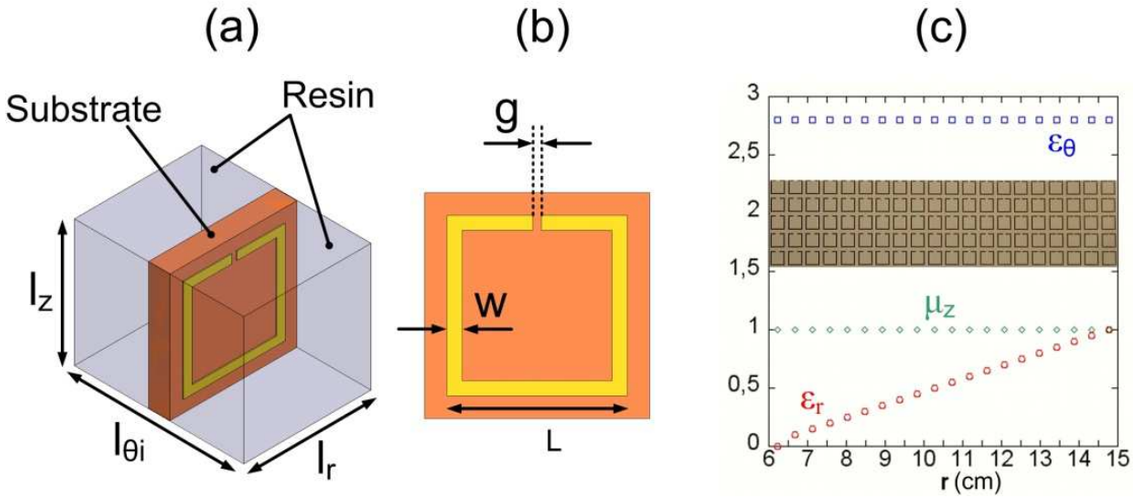

Fig. 6. (a) Unit cell. (b) The dimensions of a typical square SRR are: L=3.6 mm, w=0.3 mm and copper thickness t=35 μm. The SRRs gap g and $l_{\theta i}$, are the only varying parameters. $l_{\theta i}$ linearly decreases from the outer to the inner boundary of the cloak.

Fig. 7. (a) Realized metamaterial cloaking device (b) Picture of a portion of the experimental setup with the loop antenna mapping the magnetic field at the bottom surface of the cloak.

structure, it is difficult to access the internal field. Instead, the bottom surface of the cloak (see Fig. 8d) has been scanned taking profit of the continuity of field at this boundary in quasi-contact mode. The first measurement maps the magnetic field of the free space radiation from the horn antenna (Fig. 8(a)). The second and third measurements use a metallic cylinder alone (diameter 12 cm) (Fig. 8(b)) and surrounded with the cloak (outer diameter 30 cm) (Fig. 8(d)). The results are presented in Fig. 8 (real part of the complex transmission). The quasi-cylindrical wave output from the horn antenna is nicely resolved in our measurement (Fig. 8(a)). In presence of the metallic cylinder, the scattering and shadowing effects can be clearly observed in Fig. 8(b) as well as interferences between the

incident and reflected beams. Fig. 8(d) shows that in the presence of the cloak, the shadowing effect of the metallic cylinder is suppressed and the wave fronts are maintained thus demonstrating the cloaking effect. For comparison, simulation result using commercial finite element code (Comsol Multiphysics) for a cloak with the reduced parameters of equations [Kante, 2009]. is reported in Fig. 8(c). The fact that a non-zero field is detected in the central region of Fig. 8(b) and 8(d) results from radiation leakage below the metallic cylinder in our measurements. More importantly, the bending and redirection of quasi-cylindrical wave fronts inside the cloak can be nicely observed as a change in the radius of the horn antenna waves fronts in Fig. 8(d).

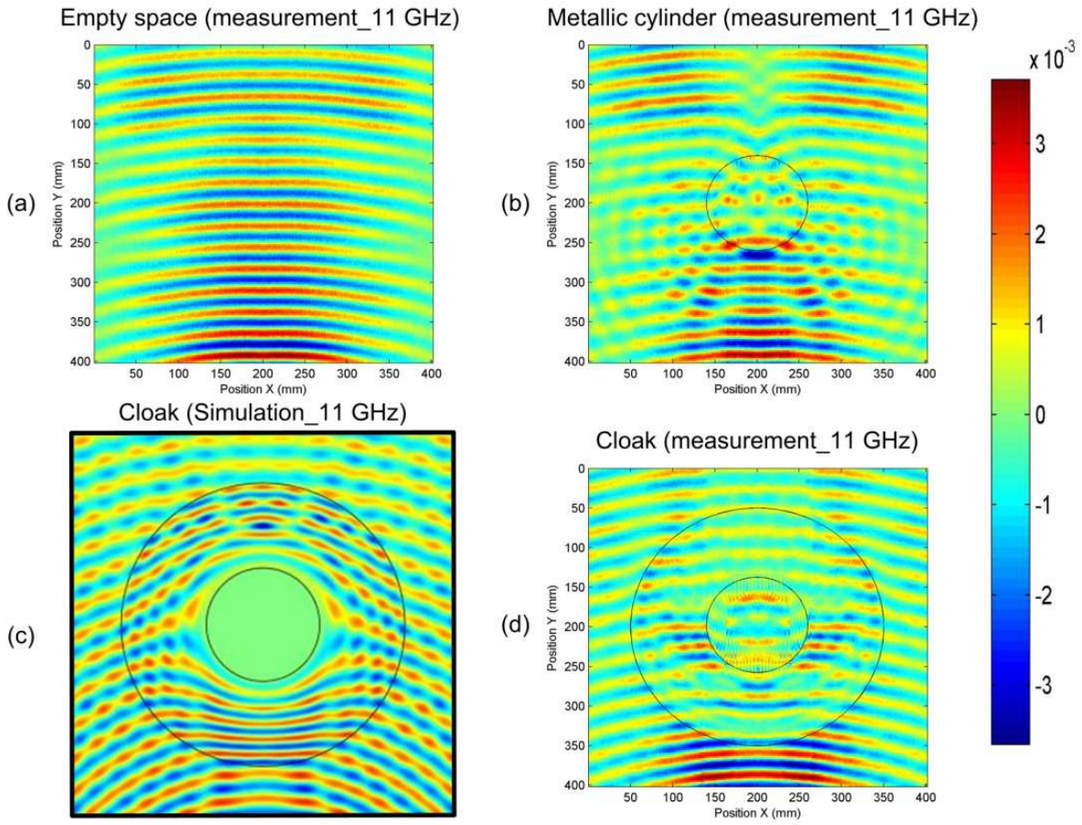

Fig. 8. Real part of the measured magnetic field output from the horn antenna in free space (a) with the metallic cylinder alone (b) and with the cloak surrounding the metallic cylinder (d). Finite element simulation exciting the cloak by the appropriate optical excitation (Comsol Multiphysics) with the reduced set of parameters presented in equations (1) is reported for comparison (c). In all cases, the 11 GHz wave travels from bottom to top.

3.4 Optical cloaks

3.4.1 Propositions of V. Shalaev

In the reference [Cai, 2008], V. Shalaev proposes two possible achievements of cloaks in the infrared and visible domains with a TE and TM polarization (figure 9).

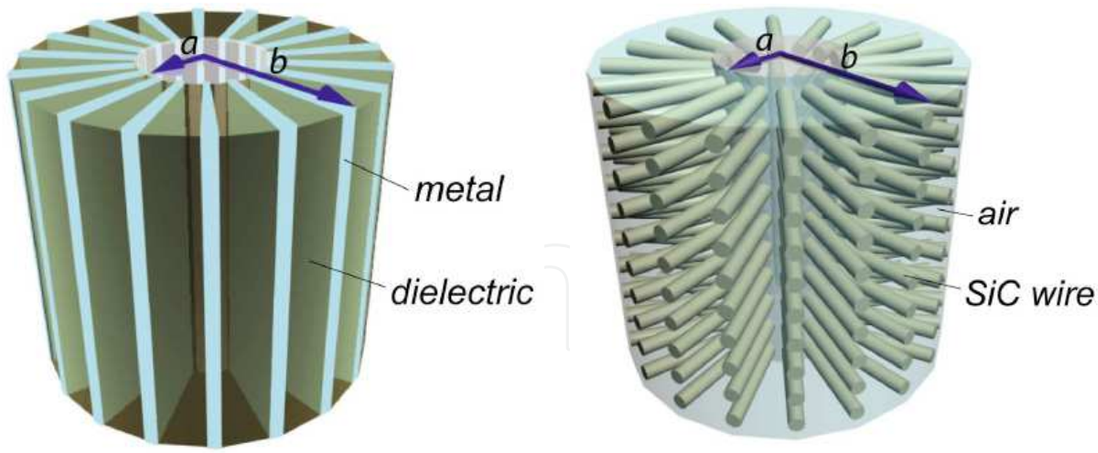

Fig. 9. Proposition of an invisibility cloak for a TE polarization (a) and a TM one (b).

The first one corresponds to a TE polarization. For this polarization, the main parameters are:

$$\varepsilon_r = \left(r'/r\right)^2 \; : \; \varepsilon_\theta = \left(\partial g(r')/\partial g(r)\right)^{-2} \; : \; \mu_z = 1 \tag{10}$$

Instead for the TM polarization the main parameters are:

$$\mu_r = \left(r'/r\right)^2 \left(\partial g(r')/\partial g(r)\right)^2 \; : \mu_\theta = 1 : \; \varepsilon_z = \left(\partial g(r')/\partial g(r)\right)^{-2} \tag{11}$$

In these expressions g(r) is the relation between the intial space and the final one. For example in the case of a cylindrical cloak :

$$r = g(r') = (1 - a / b)r' + a \tag{12}$$

In the case of a TM polarization, where ε must vary between the inside and outside of the cloak, Shalaev proposes to use an effective permittivity given by Wiener relations, varying between the permittivity of a metal (in this case silver or silicon carbide) and that of a dielectric, which can vary with the wavelength of work (like silica or barium fluoride) (Figure 9(a)).

For the TE polarization, where the permeability must vary, the material used can be silicon carbide with the shape of rods embedded in air, which seems to be a bit unrealistic at visible wavelengths. However no practical realization has been proposed.

3.4.2 Other optical cloak for TE polarization

In reference [Kante, 2008] another proposal is to use the electromagnetic properties of metal cut wires. This proposal concerns only the TE polarization, and is directly correlated to the proposed cloak in the microwave region [10] by replacing the resonators of Pendry by gold nanowires.

Indeed, the magnetic resonators of Pendry and the nanowires are equivalent for a TE polarized incident wave, where the electric field is parallel to the long side of the resonator or to the wire. The invisibility cloak that was made in the microwave domain and that operates at 11GHz can be implemented in optics by replacing the resonators used in microwave by gold nanowires (Fig. 10). This figure shows a detail of the cape made using the magnetic resonators of Pendry (Fig. 10 (a)), the simulation of the cloak at 1.5 microns (Fig. 10 (b)), a gold nanowire for a TE polarization of the incident wave (Fig. 10 (c)), the equivalent parameters of the nanowire around its first resonance frequency (Fig. 10 (d)), and a schematic view of the cape in which the resonators are replaced by gold nanowires.

3.5 Cloak with arbitrary shapes

The principles used in the cylindrical cloaks described above can be generalized to a variety of different shapes. The figure below is taken from reference [Nicolet, 2008] where a Fourier expansion is used to access to convex shapes. Reference [Rahm, 2008] proposes a square cloak (Figure 12a), which has been generalized to a polygonal cloak in [Tichit, 2008] (Figure 12b), then to an elliptical one (Figure 12c).

3.6 Broadband cloak

The major disadvantages of the first invisibility cloak were the narrow frequency-operating band and the extreme values of electromagnetic parameters needed. Various attempts have then been proposed to achieve broadband cloaks, or to design cloaks with more realistic parameter values. The most amazing proposition was suggested by U. Leonhardt who proposed to benefit from a non-Euclidean geometry to achieve the broadband [Leonhardt, 2009]. A. V. Kildishev also proposed an approximate solution to achieve a broadband cloak [Kildishev, 2008]. Following the preceding reference, we show the transition from a two-dimensional "conventional" cloak (Figure 13a) to a non-Euclidean one, namely a sphere replacing a single circle (Figure 13b). In the broadband cloak proposed by Shalaev, the principle is simple: light follows a different path depending on the operating frequency (Figure 13c).

Recently other concepts of broadband invisibility cloaks based on the use of broadband non-resonant metamaterials have been proposed [Qiu, 2009, Feng, 2011] (figure 14). These recent works are based on the use of materials made of broadband dielectric multilayer where the electromagnetic parameters are extracted using the relations of Wiener on one-dimensional multi-layer materials. Figure 14 shows an example of a dielectric multi-layer structure used in a cylindrical invisibility cloak. Each concentric layer is constituted by a sub-layer of permittivity ε_A and a sub-layer of permittivity ε_B and η is the thicknesses ratio of the two layers. The effective permittivity parameters of the layer are given by:

$$\varepsilon_\theta = \frac{\varepsilon_A + \eta\varepsilon_B}{1+\eta}, \quad \frac{1}{\varepsilon_r} = \frac{1}{1+\eta}\left(\frac{1}{\varepsilon_A} + \frac{\eta}{\varepsilon_B}\right),$$

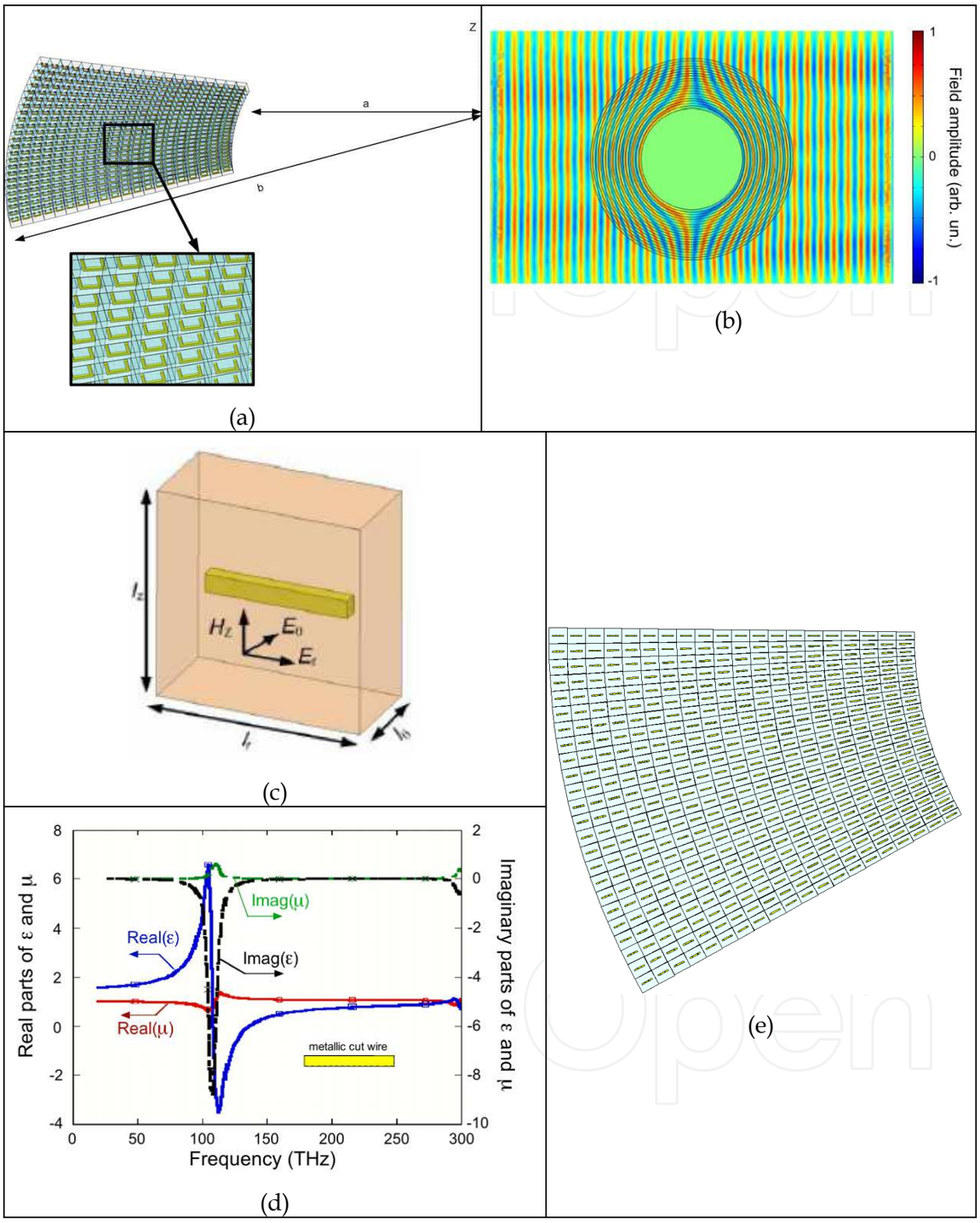

Fig. 10. (a) Cloak made of resonators of Pendry for the TE polarization of the incident field. (b) Simulation of this cloak at 1.5µm. (c) gold nanowire in TE polarization. (d) Variation of the effective permittivity and permeability of the wire as a function of frequency for a nanowire with 300nm length and a width and height of 50 nm on silicon. (e) Portion of the infra-red cloak made by a juxtaposition of gold nanowires on silicon.

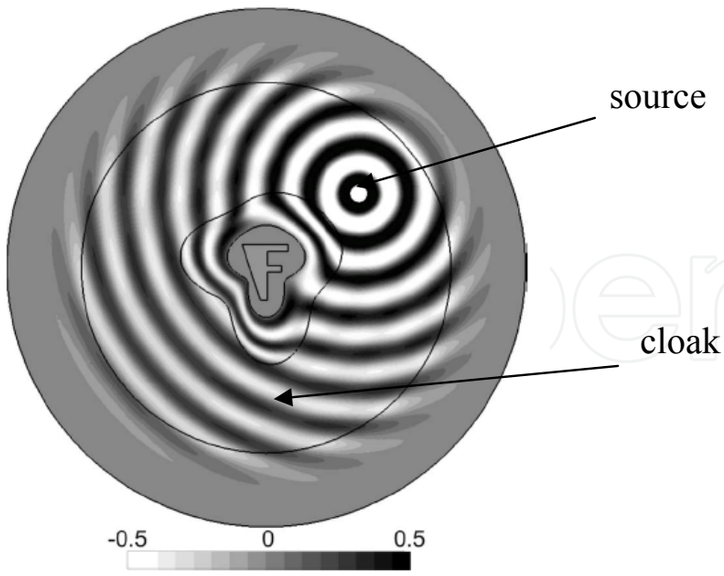

Fig. 11. Electric field radiated by a point source illuminating a cloak whose the shape is obtained by Fourier expansion of a simpler one.

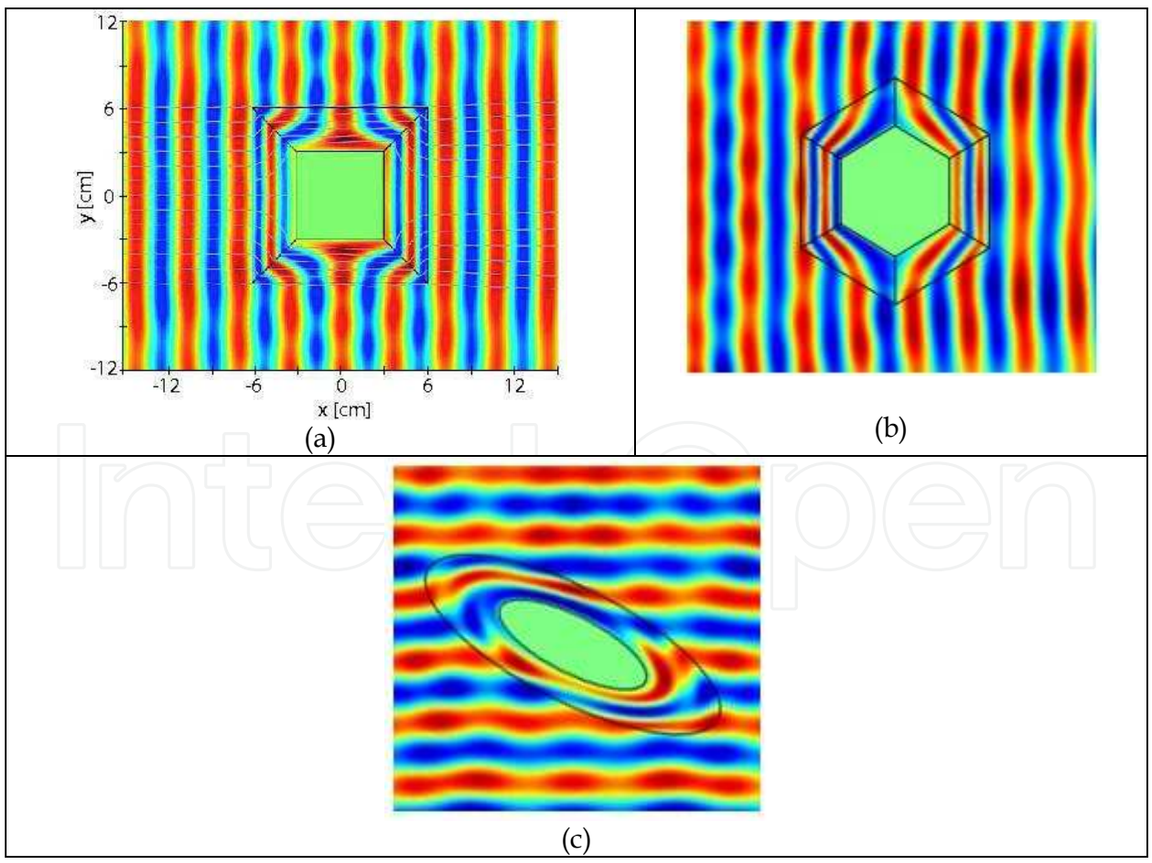

Fig. 12. (a) Squared invisibility cloak [Rahm, 2008]. (b) polygonal cloak [Tichit, 2008]. (c) elliptical cloak [Tichit, 2008].

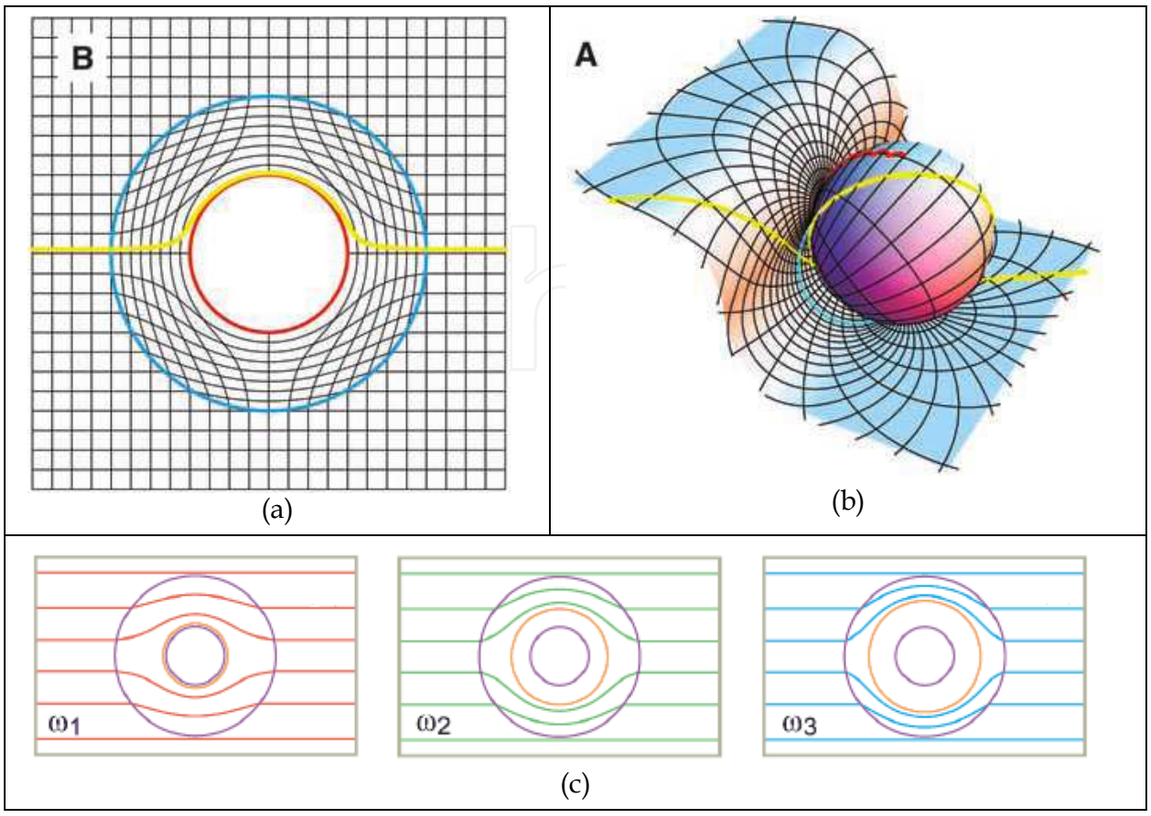

Fig. 13. (a) Classical cylindrical cloak. (b) Cloak in a non-Euclidian space. (c) Principle of the broadband cloak proposed by Shalaev : the light path changes following the frequency.

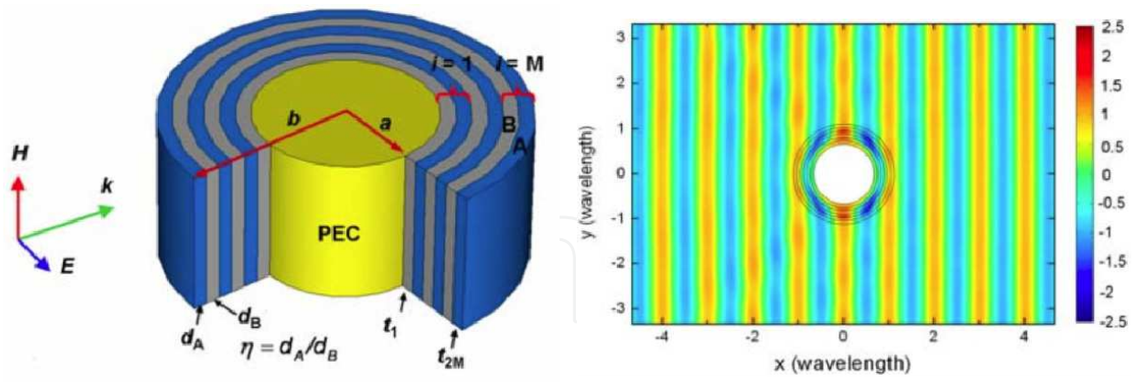

(a) (b)

Fig. 14. (a) TM plane wave incident on a PEC cylinder surrounded by concentric multilayers. The inner and outer radii of the shell are a and b, respectively. (b) The total magnetic field distribution for an optimized six-layer cloak.

A TM plane wave is incident on a PEC cylinder surrounded by concentric multilayers as shown in Fig. 14a. The inner and outer radii of the shell are *a* and *b*, respectively. The total magnetic field distribution for an optimized six-layer cloak is presented in Fig. 14b. The

main difficulty in this kind of design is the realization of permittivity lower than 1. This 2D approach was also generalized to a 3D cloak [Qiu, 2009].

3.7 Acoustic cloak

The transposition of the concept of electromagnetic cloak in acoustics has been proposed by several research laboratories in 2007 and 2008 [Torrent, 2007, Chen, 2007, Fahrat, 2008, Cummer, 2008], and particularly by the Fresnel Institute at University of Marseille. The variables considered here are the scalar pressure p, the fluid velocity, the density ρ_0, the tensor density and modulus of the fluid density λ. As for the electromagnetic cloak, we have a variation of the above parameters in spherical coordinates as in the set of equations (13) where ρ_r and ρ_ϕ are the components in the plane of the relative bulk density ρ, relative to ρ_0. This example shows the versatility of the concept that can be applied to all media where a wave can propagate.

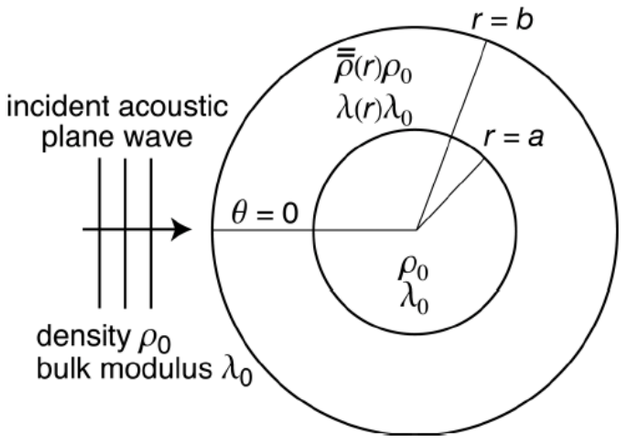

(a)

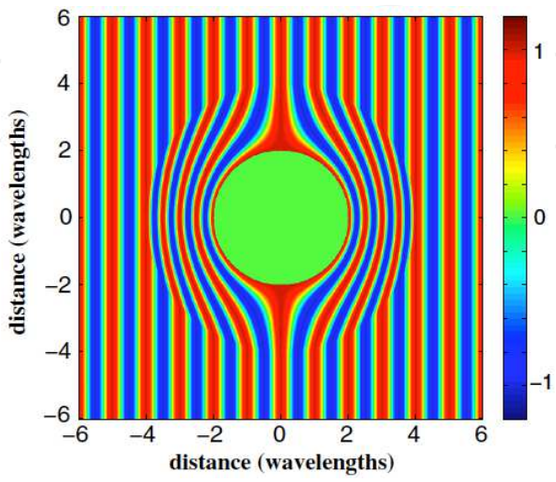

(b)

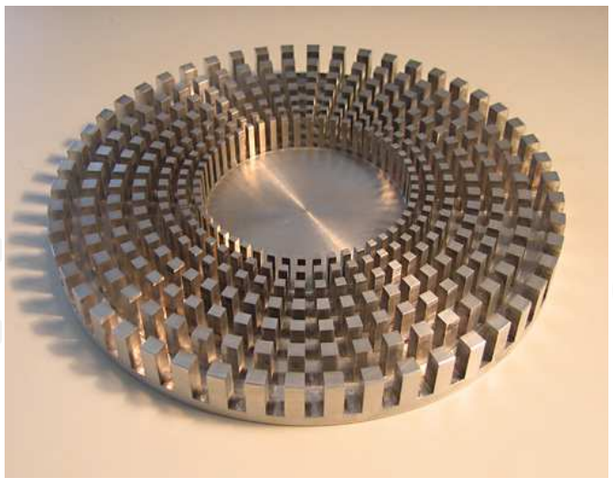

(c)

Fig. 15. (a) The principle of acoustic cloak proposed in [Cummer, 2008]. (b) Real part of the fluid pressure around the object. (c) The cloak proposed in [Fahrat, 2009].

$$\rho_\varphi = \rho_\theta = \frac{b-a}{b}$$
$$\rho_r = \frac{b-a}{b}\frac{r^2}{(r-a)^2} \tag{13}$$
$$\lambda = \frac{(b-a)^3}{b^3}\frac{r^2}{(r-a)^2}$$

4. Others applications of the space coordinate transformation

4.1 Antennas

The space coordinate transformation was proposed initially by J. Pendry and U. Leonhardt to design invisibility cloaks. This transformation of space was then used to design new devices including microwave antennas. The principle of these antennas is as follows: we define an initial space in which there is an emitter and a transformed space connected by a geometric transformation to the original space. The transformed space is realized to control the field emitted outside by the antenna. The new coordinates of the transformed space x ', y' and z 'are expressed in terms of x, y, z of the initial space

$$x'=x'(x,y,z),\ y'=y'(x,y,z),\ z'=z'(x,y,z) \tag{14}$$

Then we calculate the electromagnetic parameters of the transformed space

$$\overline{\overline{\varepsilon'}} = \overline{\overline{J}}\,\overline{\overline{\varepsilon}}\,\overline{\overline{J}}^{T}\,(\det \overline{\overline{J}})^{-1} \quad \overline{\overline{\mu'}} = \overline{\overline{J}}\,\overline{\overline{\mu}}\,\overline{\overline{J}}^{T}\,(\det \overline{\overline{J}})^{-1} \tag{15}$$

where $\overline{\overline{\varepsilon}}$ is the permittivity tensor, $\overline{\overline{\mu}}$ the permeability tensor and $\overline{\overline{J}}$ the Jacobian matrix defined by

$$\overline{\overline{J}} = \frac{\partial(x',y',z')}{\partial(x,y,z)} = \begin{pmatrix} \partial x'/\partial x & \partial x'/\partial y & \partial x'/\partial z \\ \partial y'/\partial x & \partial y'/\partial y & \partial y'/\partial z \\ \partial z'/\partial x & \partial z'/\partial y & \partial z'/\partial z \end{pmatrix} \tag{16}$$

In the initial space, an antenna emits a certain type of radiation. This radiation is then modified by the transformation of the space in which it propagates. Several examples have been proposed in recent papers [Kong,2007, Tichit, 2009, Tichit, 2011, Rui, 2011, Cui 2011].

4.1.1 1st example: Parabolic transformed antenna

An example of a directional antenna is given below [Kong, 2007], where a parabolic space is transformed into a rectangular one (Figure 16a). In this example we are in TM polarization.

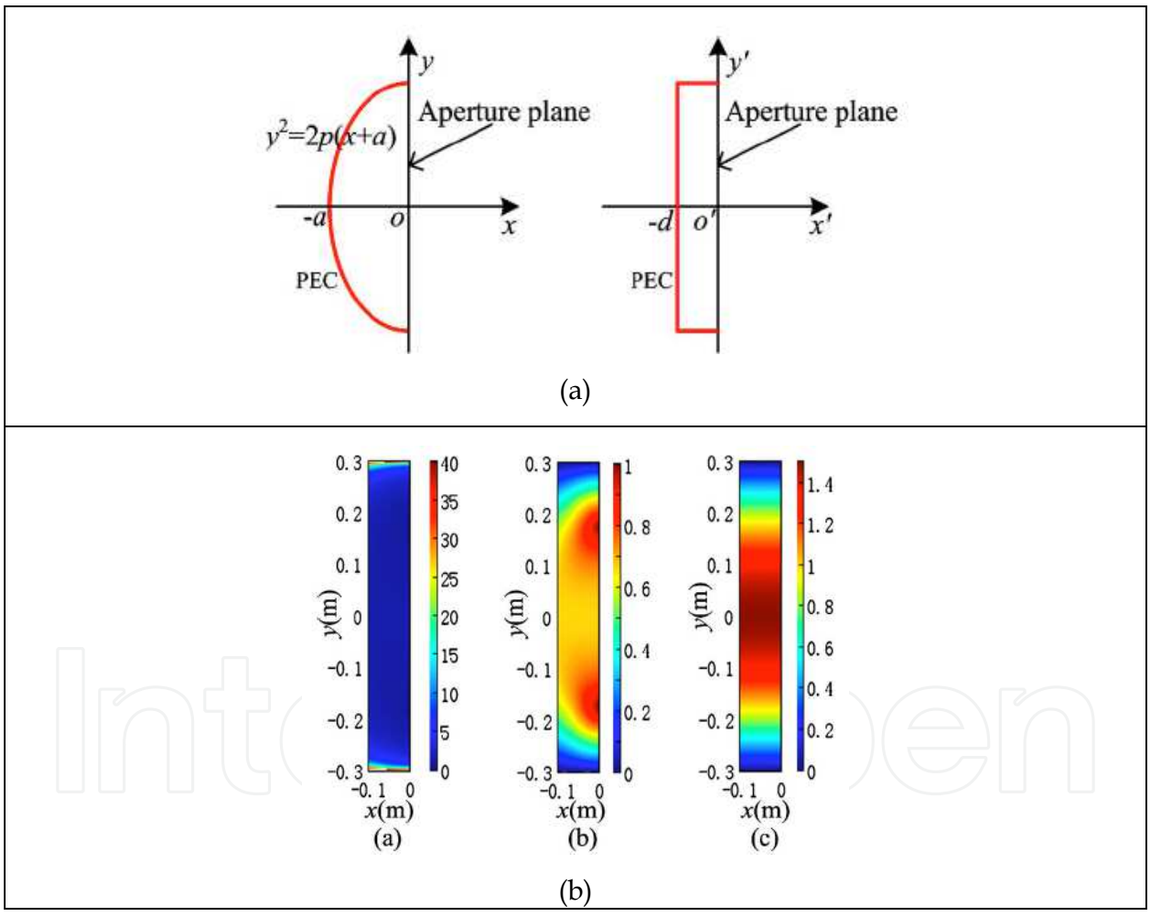

Fig. 16. (a) Initial parabolic space and transformed rectangular space. (b) Variation of the electromagnetic parameters μ_x, μ_y et ε_z of the transformed space.

Figure 16b shows the variations of the calculated electromagnetic parameters. Figure 17 shows the radiation of a horn in the transformed space. In this example, the benefit of the transformation of space is not real in the sense that the obtained antenna has almost the same size as the original antenna. Moreover, in this reference, the antenna has not been

realized and the far-field radiation patterns have not been presented. However, space coordinate transformation can be used to design antennas more compact than conventional ones. This is the case of the antenna proposed theoretically in reference 23 and experimentally measured in [Tichit, 2009].

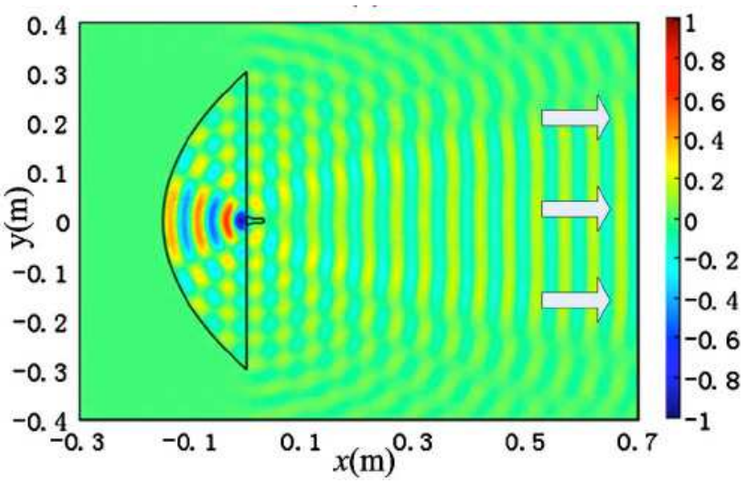

(a)

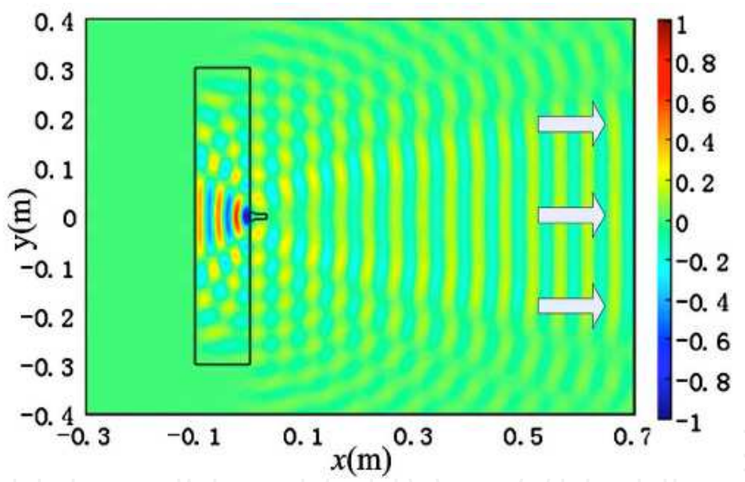

(b)

Fig. 17. (a) Horn antenna emitting in the parabolic space. (b) horn antenna emitting in the transformed space. In both cases the near fields are almost equivalent.

4.1.2 2nd example: Directive antenna

The 2nd example concerns the transformation of an isotropic antenna into a directive one [Tichit, 2009, Tichit, 2011]. This isotropic antenna is taken as an infinite radiating wire. The initial space is then supposed to be the cylindrical space surrounding the wire. The transformed space is a rectangular one as illustrated in Figure 18. After the transformation, the radiating wire in the cylindrical space is then comparable to a plane source radiating in the rectangular space.

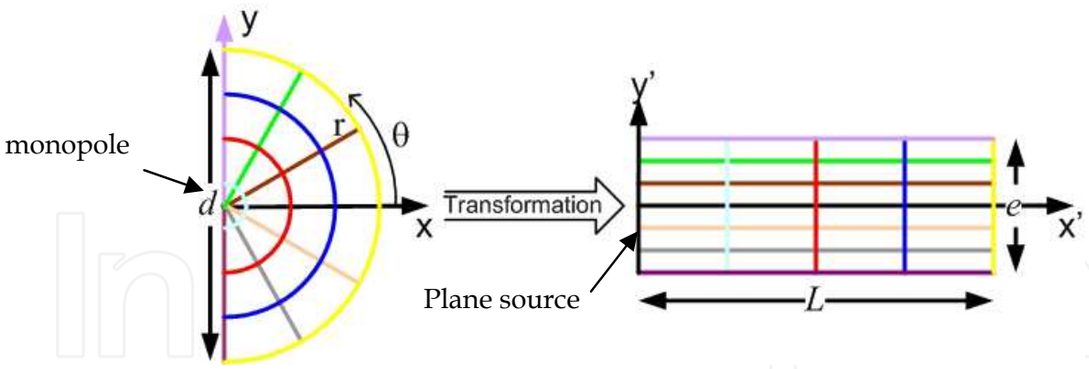

Fig. 18. Initial cylindrical space with the radiating monopole (left) and the transformed space (right) with the transformed plane source.

Figure 19 shows the variations of the electromagnetic parameters ε_{xx}, ε_{yy}, *and* μ_{zz} needed to achieve the space transformation. The expressions of these parameters are as follows:

$$\overline{\overline{\varepsilon}} = \begin{pmatrix} \varepsilon_{xx}(x',y') & 0 & 0 \\ 0 & \varepsilon_{yy}(x',y') & 0 \\ 0 & 0 & \varepsilon_{zz}(x',y') \end{pmatrix} \varepsilon_0 \qquad \overline{\overline{\mu}} = \begin{pmatrix} \mu_{xx}(x',y') & 0 & 0 \\ 0 & \mu_{yy}(x',y') & 0 \\ 0 & 0 & \mu_{zz}(x',y') \end{pmatrix} \mu_0 \quad (17)$$

with

$$\varepsilon_{xx}(x',y') = \mu_{xx}(x',y') = \frac{\pi}{e}x' \qquad \varepsilon_{yy}(x',y') = \mu_{yy}(x',y') = \frac{1}{\varepsilon_{xx}(x',y')} \quad (18)$$

where d, e and L are the geometrical dimensions of the initial and transformed spaces.

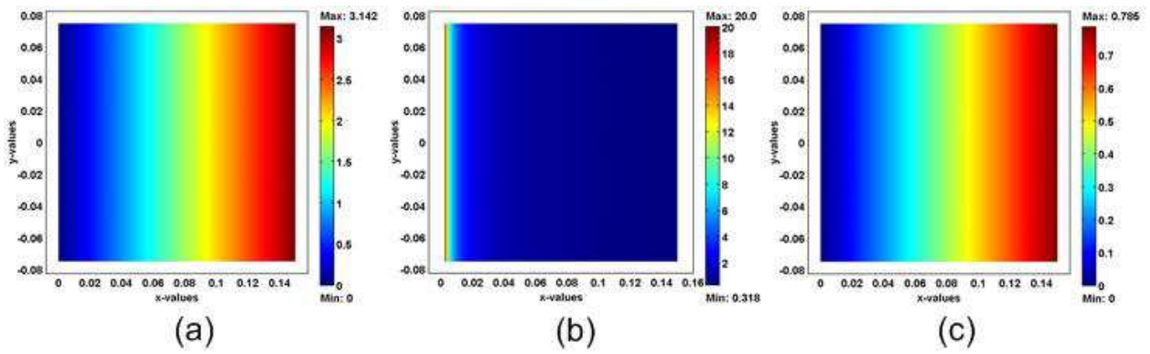

Fig. 19. Variations of the electromagnetic parameters of the transformed space: (a) ε_{xx}, (b) ε_{yy}, et (c) ε_{zz}.

The expressions of the electromagnetic parameters vary continuously, and remain limited to reasonable values. Figure 20 shows the calculated magnetic field at 5, 10 and 40 GHz. The directivity of the antenna increases as the frequency rises. The dimensions of the antenna are shown in Figure 20a. One can observe that there is no reflection between the metamaterial and the air.

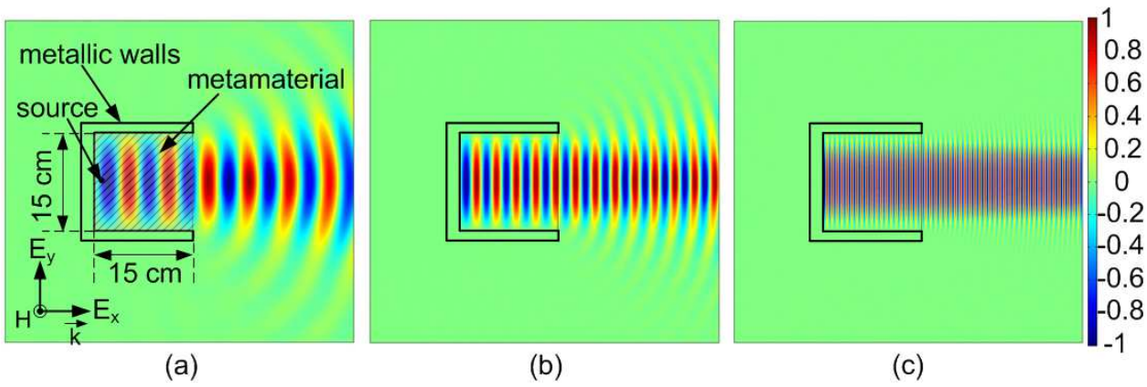

Fig. 20. Magnetic field cartography for a TM wave polarization calculated at (a) 5, (b) 10 and (c) 40 GHz.

The practical realization of this antenna, however, requires a simplification of these parameters. One solution proposed recently is to use a discrete variation of these parameters. The simplification is performed with a conservation of the propagation equation. The following set of parameters is then obtained:

$$\varepsilon_{yy} = \mu_{zz} = 1 \; : \; \varepsilon_{xx} = \left(\frac{\pi x}{e} \right)^2 \tag{19}$$

The material needed must have a variable permittivity in the direction of propagation Ox. The other parameters remain constant. Figure 21a shows a detail of the material used to make the variable permittivity, and the fabricated antenna prototype for an operation near 10 GHz. Figure 21b shows the performances of this antenna. It can be observed that the radiation pattern of the antenna is not affected by the simplification and the discretization of the material.

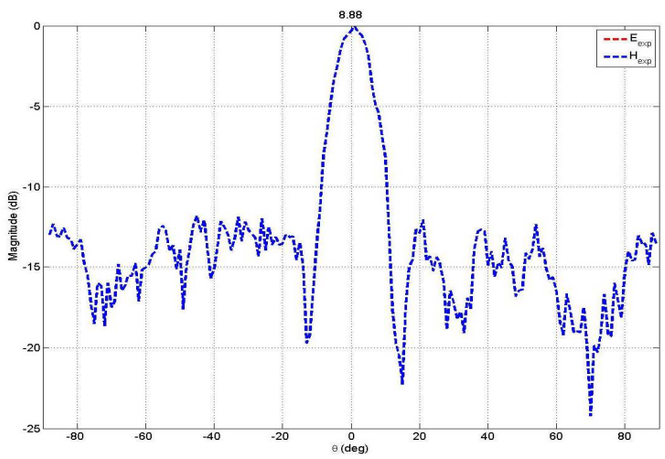

(a)

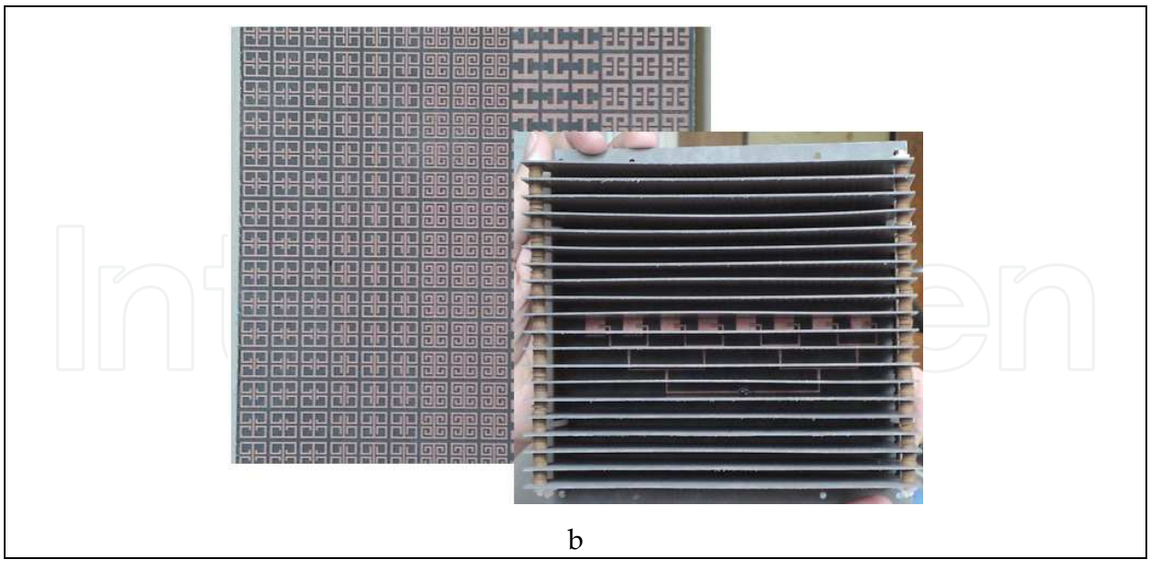

b

Fig. 21. (a) Normalized measured radiation pattern of the antenna. (b) detail of the metamaterial and of the realized antenna.

4.1.3 3rd example: Broadband Fresnel antenna

The previous antenna made use of resonant metamaterials. Then its bandwidth is inherently narrow. An interesting broadband operation proposal was recently presented by Y. Hao [Rui, 2011]. A broadband Fresnel lens can be realized using a multilayer dielectric structure. The permittivities of the different layers are calculated using space coordinate transformation. Figure 22 shows an example of such antenna. The performances are presented in part II of the figure. We can note the broadband characteristics of the antenna in IId.

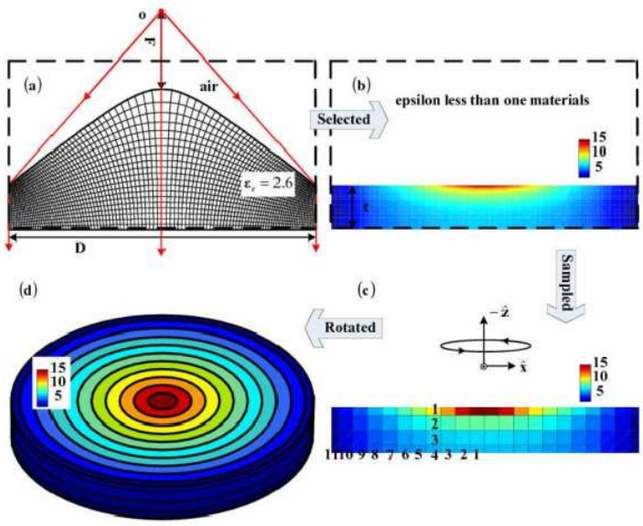

I

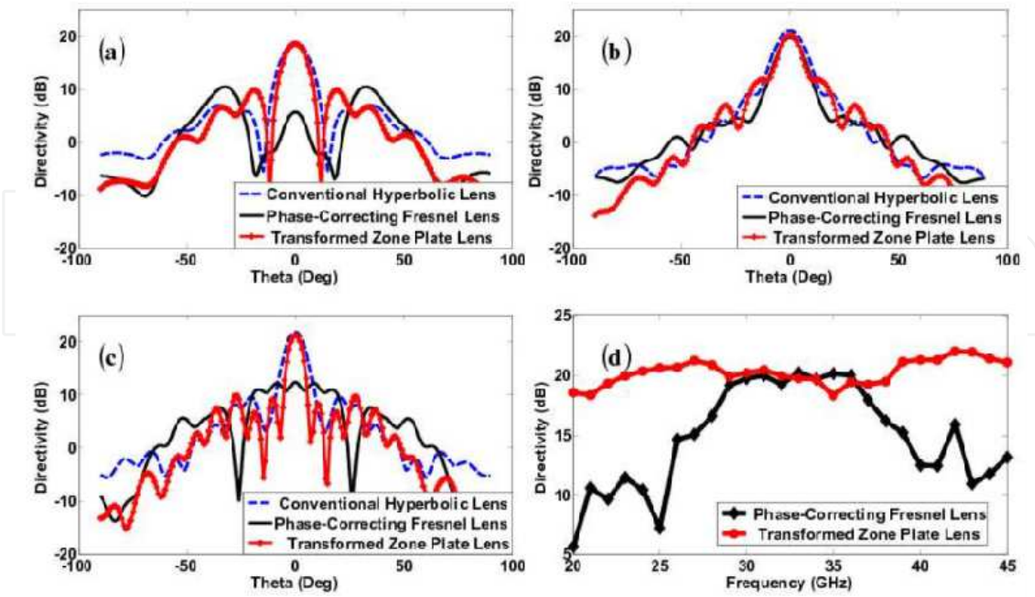

II

Fig. 22. I/ Schematic showing of the transformed zone plate lens antenna. (a) 2D hyperbolic lens with nearly orthogonal mapping. (b) 2D flat lens with the permittivity map consisting of 110×20 blocks. (c) 2D flat lens with the permittivity map consisting of 22×4 blocks. (d) 3D transformed zone plate lens antenna. II/ The radiation patterns of the conventional 3D hyperbolic lens, 3D phase-correcting Fresnel lens and 3D transformed zone plate lens at (a) 20 GHz, (b) 30 GHz, (c) 40 GHz. (d) The comparison of the bandwidth performance of 3D phase-correcting Fresnel lens and 3D transformed zone plate lens from 20 GHz to 45 GHz

4.1.4 4th example: Three-dimensional metamaterial lens antennas

The proposal of T.J. Cui to realize a lens using variable index material so as to focalize the beam of a waveguide is also an interesting application of transformation optics [Cui, 2011]]. Figure 23 shows a photo of the realized prototype and the performances of this lens in X band. The antenna presents two main advantages: the broadband behavior of the dielectric and the easiness of the realization (at microwave frequencies). Indeed the index gradient is realized with an array of variable size closed square rings printed on a dielectric substrate. Remains the classical drawback of the impossibility to realize an index lower than 1.

4.2 Circuits

M. Rahm proposed in [Rahm, 2008] a general method to achieve an invisibility cloak. But he also proposed the implementation of energy concentrator. Figure 24a shows a simulation of such a device. In [Lin, 2008], L. Lin proposed a number of applications such as a phase transformer to transform a cylindrical wavefront to a plane wavefront (Figure 24b) or a power divider (Figure 24c). In [Huangfu, 2008], J. Huangfu proposed a method to achieve wave guiding without reflection at 90° bends (Figure 24d).

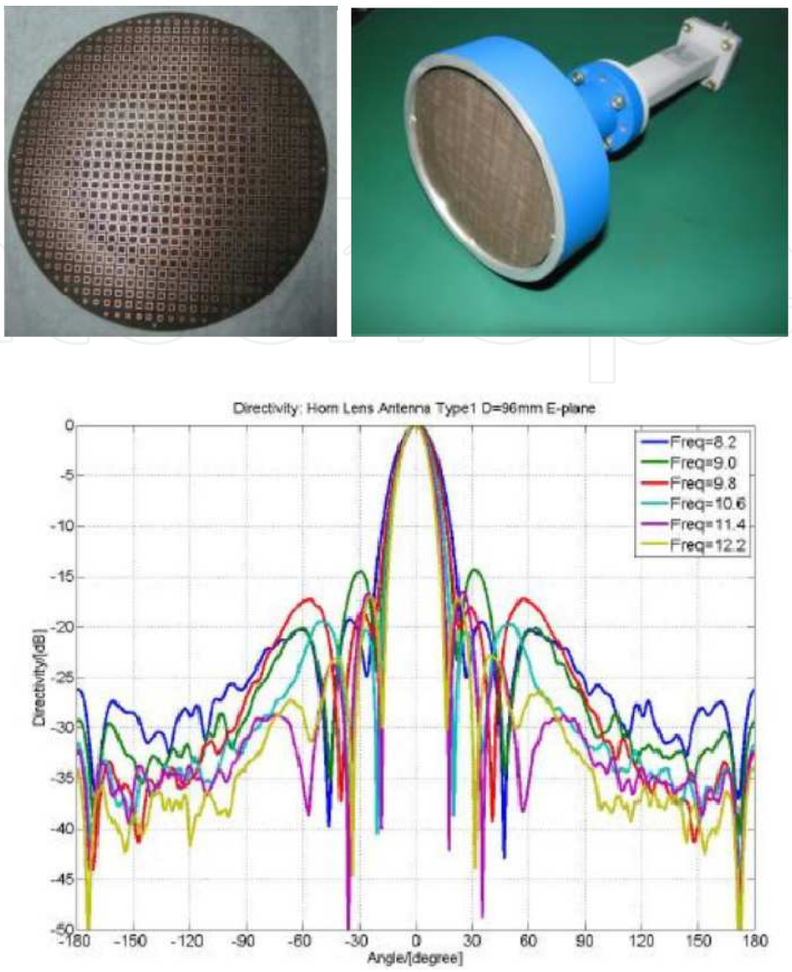

Fig. 23. (a) The 3D flat-lens antenna made of gradient index metamaterial. The aperture size is 9.6 cm. (b) The measured far-field radiation patterns of the 3D metamaterial flat lens antenna in the X band.

Other devices were recently proposed in the domain of the optical waveguiding devices [Ghasemi, 2010, Liu, 2008]. The proposal in [Ghasemi, 2010] tends to answer to a main drawback of use of metallic metamaterials at optical frequencies which is their high losses. A promising approach consists in creating hybrid photonic structures in which metallic parts are coupled with dielectric (and almost lossless) waveguides. In this configuration, useful functionalities are obtained by allowing just enough light to interact with the metallic parts of the system. The remaining part of the energy propagates in the dielectric waveguide, thereby considerably mitigating the losses. Figure 25 shows a mode adapter designed using this approach. The mode adapter allows the transition of the energy flow from a large SOI ridge waveguide to a narrower one. The taper has been achieved using the method of transformation optics. Although the authors simply considered a 2D transformation, they show that this structure can effectively act upon the three dimensional flow of light guided by the SOI structure.

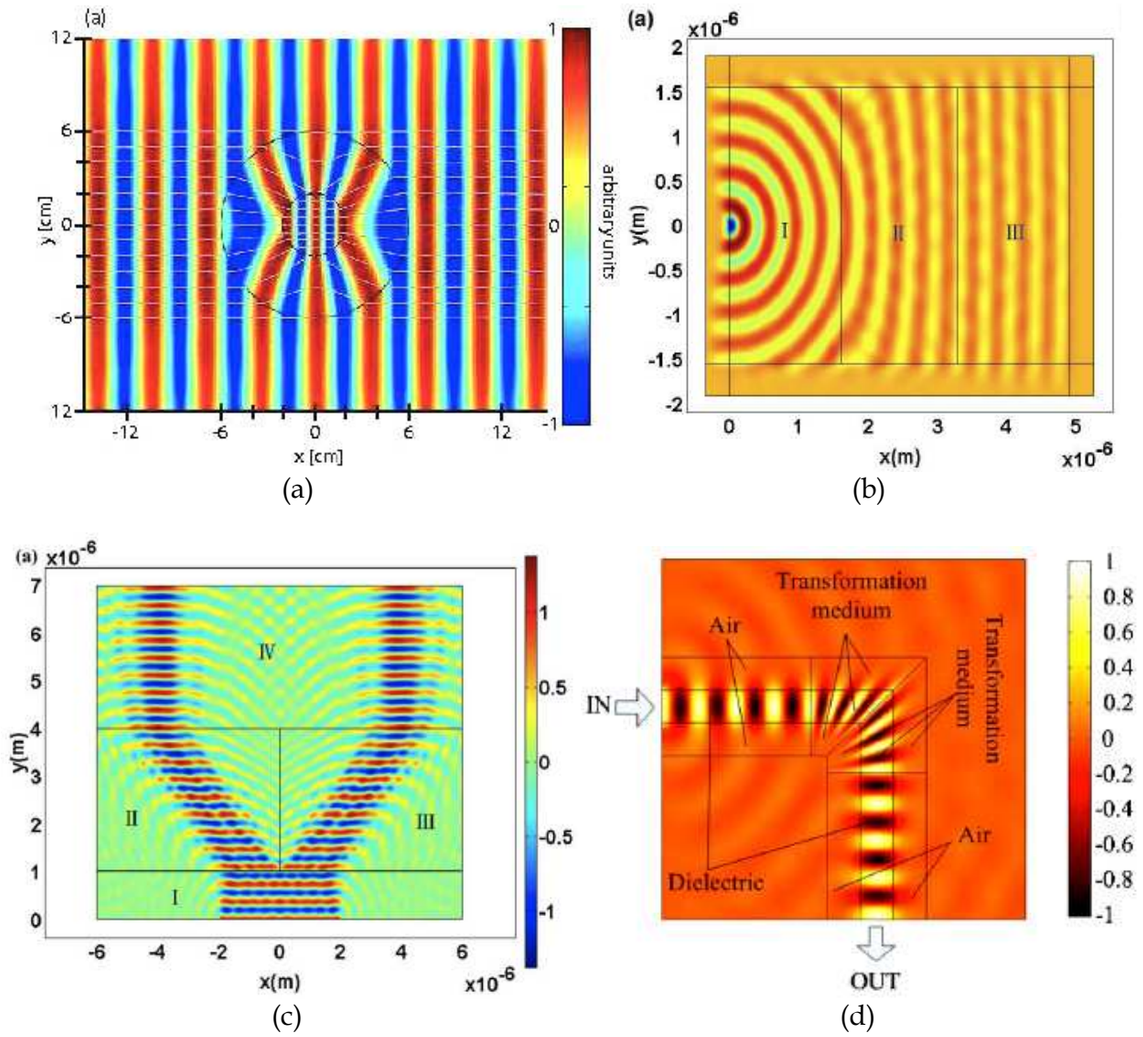

Fig. 24. (a) Energy concentrator proposed in the reference 12. (b) Phase Transformer between 2 regions. (c) Power divider. (d) 90° waveguide bend without loss.

4.3 Broadband carpet cloak

4.3.1 Microwave broadband carpet cloak

D. R. Smith has recently proposed a broadband cloak that can be adjusted to any object placed on the ground [Valentine, 2009]. This cloak allows to reconstruct the reflection of light incident on an object in order to make as if the object was not present. The object must however have dimensions small compared to the dimensions of the cloak. Figure 26a illustrates the operating principle of the cloak. Figure 26b gives a picture of its implementation and shows the pattern of the material permittivity variable used. The idea is to change the optical path followed by the reflected beam. The carpet cloak reconstructs the reflected beam as it is when no object is placed on the ground. This is clearly shown in Figure 26a: in I the ground reflects an incident beam without obstacle, in II the beam is reflected in the presence of an obstacle, in III the reflected beam consists of parallel rays reconstructed by the cloak covering the obstacle.

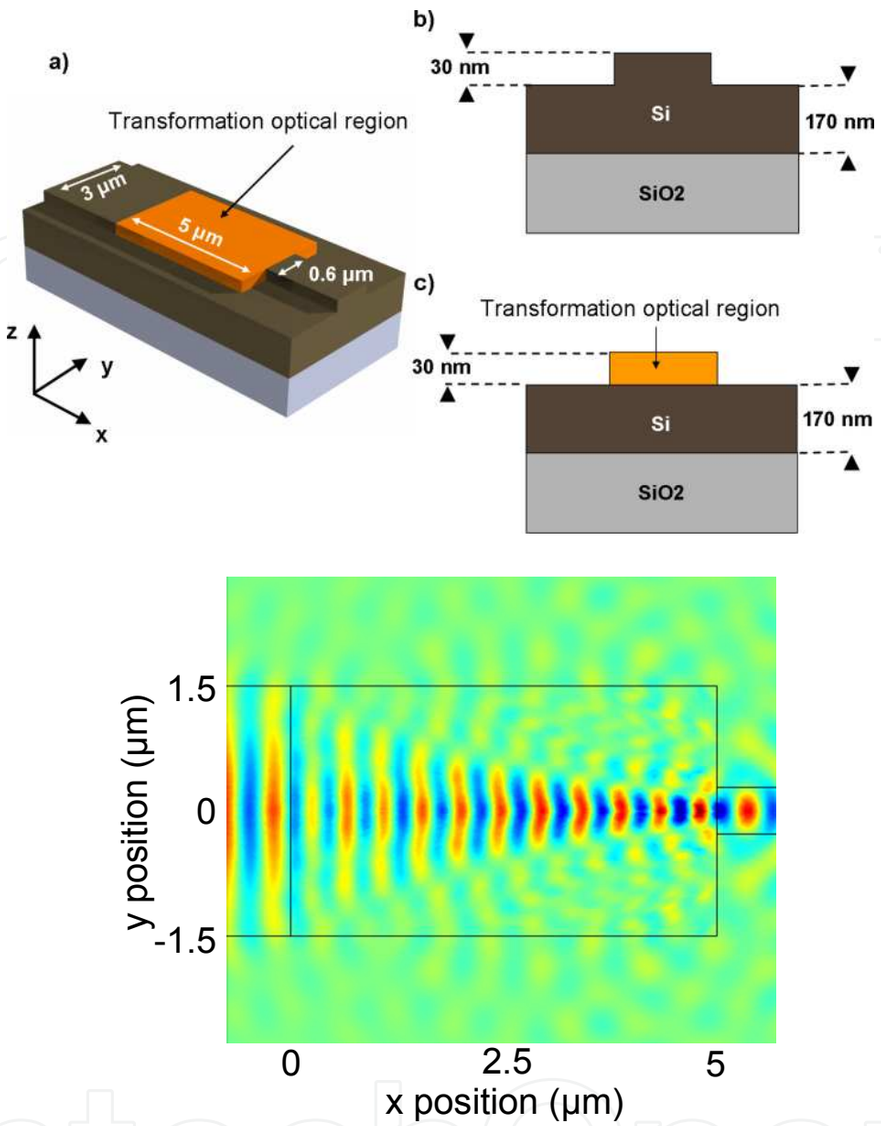

(d)

Fig. 25. (a) Geometry of the mode adapter considered in this study; (b) cross-sectional view of the input SOI ridge waveguide; (c) cross-sectional view of the mode adapter. (d) Transition from the large to the narrow waveguide using a mode adapter. The y-component of the electric field is shown in the x-y plane located halfway through the Si slab.

4.3.2 Optical carpet cloak

The same principle can be applied in infrared and visible domains [Gabrielli, 2009, Greenleaf, 2007, Cheng, 2009]. In reference [Gabrielli, 2009], the authors present the realization and the characterization of a carpet cloak operating in the optical domain. Figure 27 shows a view of the realized carpet on silicon.

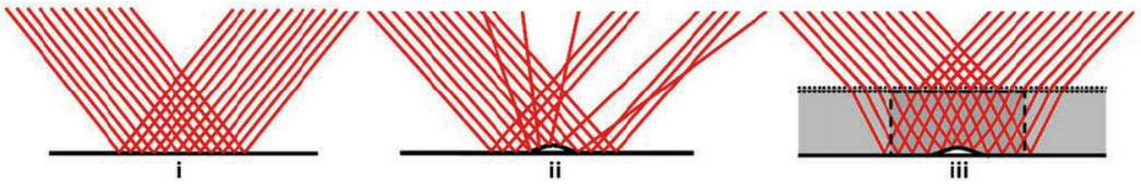

(a)

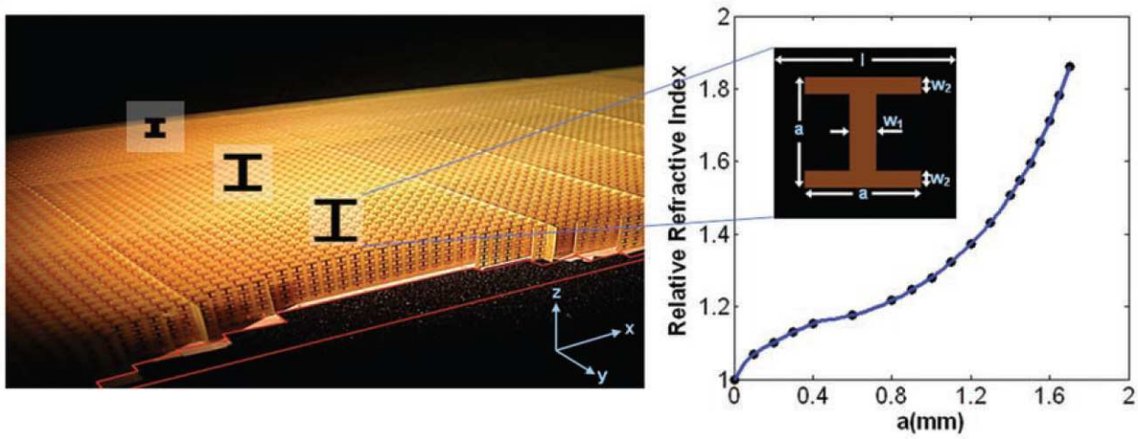

(b)

Fig. 26. Principle of the carpet cloak: in I the ground reflects an incident beam without obstacle, in II the beam is reflected in the presence of an obstacle, in III the reflected beam consists of parallel rays reconstructed by the cloak covering the obstacle. (b) View of the realized carpet cloak and the metamaterial unit cell with variable permittivity used in the carpet.

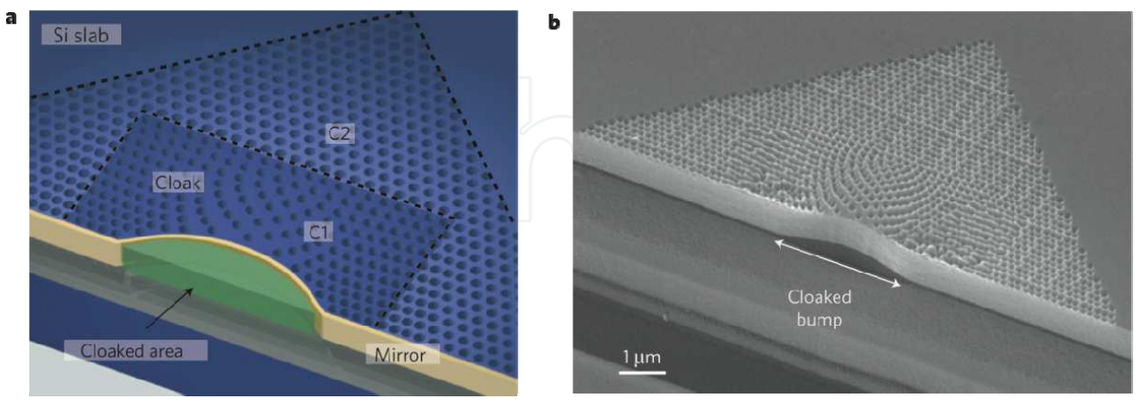

Fig. 27. Principle (a) and realization (b) of an optical carpet cloak on silicon.

Figure 28 shows the carpet cloak operating at a wavelength of 1,540 nm, for an incident Gaussian beam reflected from a curved reflecting surface. Similar reflection characteristics can be observed when compared to a reflection on a flat surface.

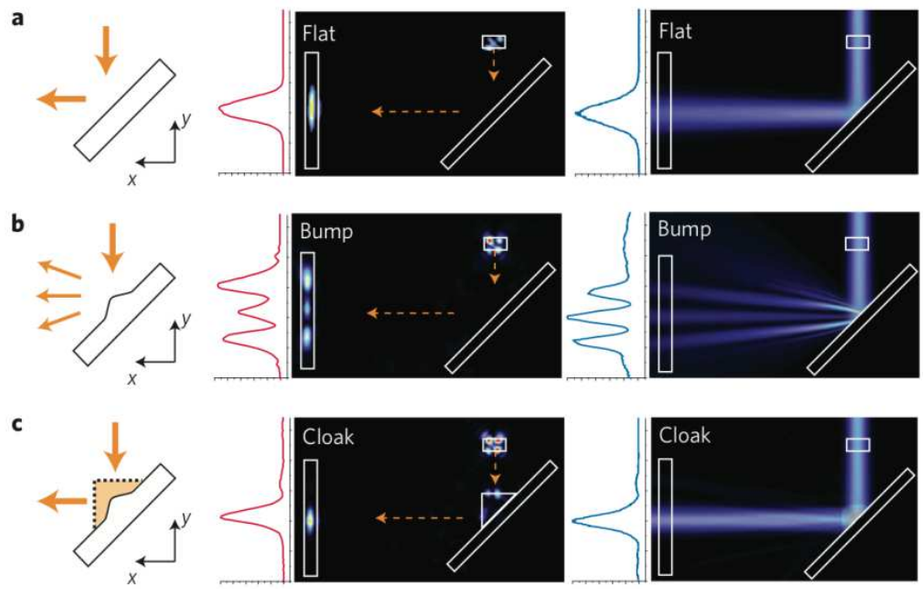

Fig. 28. Optical carpet cloaking at a wavelength of 1,540 nm: The results for a Gaussian beam reflected from a flat surface (a), a curved (without a cloak) surface (b) and the same curved reflecting surface with a cloak (c).

4.4 Electromagnetic wormhole and other cosmological objects

One of the most amazing applications has been proposed by A. Greenleaf [Greenleaf, 2007]. He imagined to create a wormhole using electromagnetic invisibility cloak able to link two remote areas of space and ensures the propagation of an electromagnetic wave between both regions invisible from the outside. Figure 29 shows a schematic illustration of the wormhole where its exterior deflects the incident electromagnetic waves and a section of the wormhole showing a wave propagating inside.

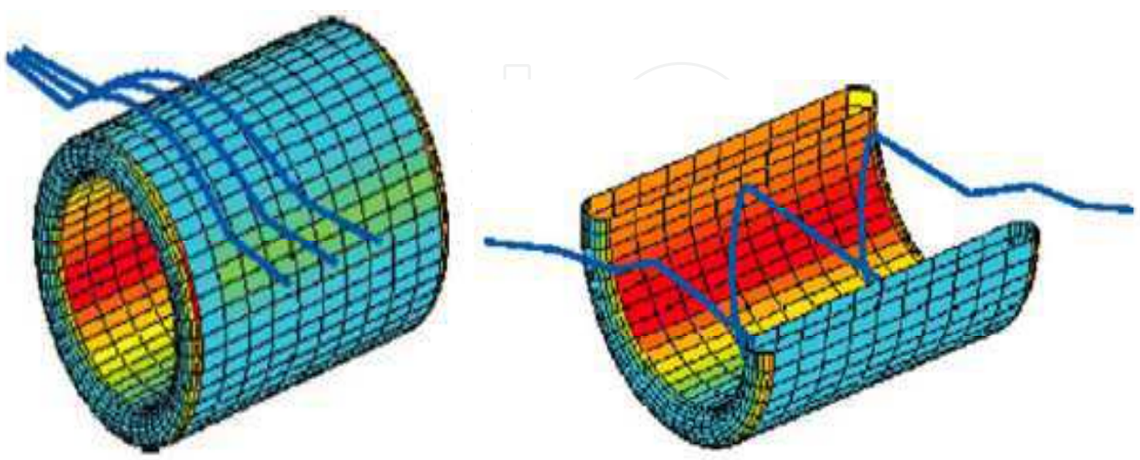

Fig. 29. (a) A schematic illustration of the wormhole whose exterior cloak deflects the incident electromagnetic waves. (b) a section of the wormhole showing a wave propagating inside.

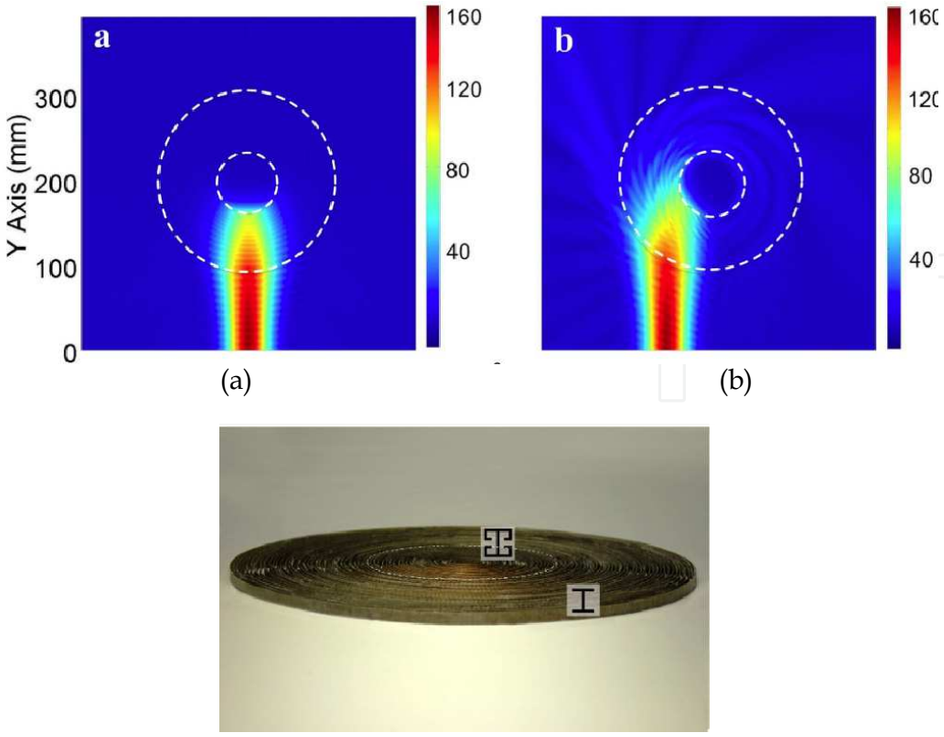

Fig. 30. (a) Distributions of electric fields |Ez| for the designed black hole at the frequency of 18 GHz: The full-wave simulation result under the on-center incidence of a Gaussian beam. (b) The full-wave simulation result under the off-center incidence of a Gaussian beam. (c) Photograph of the fabricated artificial black hole based on metamaterials, which is composed of 60 concentric layers, with ELC structures in the core layers and I-shaped structures in the shell layers.

5. Conclusion and outlooks

The potential applications of the space coordinate transformation seem to be very various. The examples presented in this chapter show their usefulness, even if they are still far from industrial achievements. Also it appears that these applications can be transposed to any frequency. The conventional metamaterials used in the microwave region are metal-dielectric structures. However metals have different present high losses at infrared and optical frequencies. Therefore the applicability will differ greatly between the microwave domain on one hand, and optical frequencies on the other. In the optical domain, the problem is mainly the achievement of materials with metallic patterns having sizes of about one-tenth of the wavelength (a few hundred nanometers) and the control of their geometry [Soukoulis, 2011]. The other problem is the losses of the metallic metamaterials at optical wavelengths. Innovative approaches have recently been proposed to solve partially this problem. But the problem is not completely solved.

In the microwave field, the achievements seem easier as they involve usually inexpensive materials, and metallic parts of the metamaterials present low losses at these frequencies. But they depend strongly on the complexity of the electromagnetic parameters to achieve. In

the rare realizations proposed in literature, these parameters have been simplified, and often the impedance matching has been sacrificed to obtain a feasible material. The metamaterial based design encountered in this case the problem of reflection losses, and are already comparable to existing solutions that have proved their performances, for example in the field of antennas. Another difficulty is the narrow bandwidth of the metamaterials used, in particular those based on resonant structures of the type of split ring resonators of Pendry. In reality this is not really a problem, because broadband metamaterials can be realized from composite metamaterials [Djermoun, 2007], or by using all dielectric structures.

6. References

Tannery P., Henry C. et de Waard C., *Œuvres de Pierre de Fermat*, Gauthier-Villars et Cie, Paris, 1891-1922.

Pendry, J. B., Schurig, D., Smith, D. R., (2006), Controlling Electromagnetic Fields, *Science,* Vol. 312, pp. 1780-1782.

Leonhardt, U., (2006), Optical Conformal Mapping, *Science,* Vol.312, pp.1777-1780.

Cai W., Chettiar U. K., Kildishev A. V., and Shalaev V. M.. (2008), Designs for optical cloaking with high-order transformations, *Optics Express,* Vol. 16, No. 8, pp.5444-5452.

Schurig, D., J. J. Mock, B. J. Justice, S. A. Cummer, J. B. Pendry, A. F. Starr, and D. R. Smith, (2006), Metamaterial Electromagnetic Cloak at Microwave Frequencies, *Science,* Vol.314, pp. 977-980

Soukoulis C.M., Wegener M., (2011), Past achievements and future challenges in the development of three-dimensional photonic metamaterials, *Nature Photonics*, Vol.5, pp.523-530

Guven K., Saenz E., Gonzalo R., Ozbay E. and Tretyakov S., (2008), Electromagnetic cloaking with canonical spiral inclusions, *New Journal of Physics*, Vol.10, 115037

Kanté B., de Lustrac A., Lourtioz J.-M., Burokur S. N., (2008), Infrared cloaking based on the electric response of split ring resonators, *Optics Express*, Vol.16, N° 12, pp.9191-9198,

Kanté B., Germain D., and de Lustrac A., (2009), Experimental demonstration of a nonmagnetic metamaterial cloak at microwave frequencies » *Physical Review B*, Vol. 80, 201104(R).

Nicolet A., Zolla F., Guenneau S., (2008), Electromagnetic analysis of cylindrical cloaks of an arbitrary cross section, *Optics Letters,* Vol.33, No. 14, pp.1584-1586.

Rahm M., Schurig D., Roberts D. A., Cummer S.A., Smith D. R., Pendry J. B., (2008), Design of electromagnetic cloaks and concentrators using form-invariant coordinate transformations of Maxwell's equations, *Photonics and Nanostructures. Fundamental and Applications,* Vol.6, 87.

Tichit P-H., Kante B., de Lustrac A., (2008) Design of polygonal or elliptical invisibility cloak, Nato Workshop Meta 08, Marrakesh, may 07-10 2008.

Leonhardt U., Tyc T., (2009), Broadband Invisibility by Non-Euclidean Cloaking, *Science,* Vol.323, pp.110-112;

Kildishev A. V., Cai W., Chettiar U. K., Shalaev V.M., (2008), Transformation optics: approaching broadband electromagnetic cloaking, *New Journal of Physics*, Vol.10, 115029.

Qiu C.-W., Hu L., Xu X., Feng Y., (2009), Spherical cloaking with homogeneous isotropic multilayered structures, *Physical Review E,* Vol.79, 047602.

Feng Y. J., Xu X. F., Yu Z. Z., (2011), Practical realization of transformation-optics designed invisibility cloak through layered structures, *Antennas and Propagation (EUCAP), Proceedings of the 5th European Conference*, pp. 3456 – 3460, ISBN: 978-1-4577-0250-1, Rome, 11-15 April 2011.

Torrent D. and Sanchez-Dehesa J., (2009), Acoustic metamaterials for new two-dimensional sonic devices, *New Journal of Physics*, Vol.9, 323 (2007).

Chen H., Chan C. T., (2007), Acoustic cloaking in three dimensions using acoustic metamaterials, *Applied Physics Letters,* Vol.91, 183518.

Farhat M. Enoch S., Guenneau S., Movchan A. B., (2008), Broadband cylindrical acoustic cloak for linear surface waves in a fluid, *Physical Review Letters* Vol.101, 134501

Cummer S. A., Popa B. I., Schurig D., Smith D. R., Pendry J., Rahm M., Starr A., (2008), Scattering Theory Derivation of a 3D Acoustic Cloaking Shell, *Physical Review Letters*, Vol.100, 024301.

Kong F., Wu B., Kong J. A., Huangfu J. H., and Xi S., (2007), Planar focusing antenna design by using coordinate transformation technology, *Applied Physics Letters,* Vol.91, 253509.

Tichit P.-H., Burokur S. N., de Lustrac A., (2009), Ultra-directive antenna via transformation optics, *Journal of Applied Phys*ics, Vol.105, 104912

Tichit P.-H., Burokur S. N., de Lustrac A., (2011), Design and experimental demonstration of a high-directive emission with transformation optics, *Physical Review B,* Vol.83, 155108.

Rui Y., Wenxuan T., Hao Y., (2011), Broadband Dielectric Zone Plate Antenna from Transformation Electromagnetics, *Optics Express,* Vol.19, n°13, pp.12348-12356.

Cui T. J., Zhou X. Y., Ma H. F., (2011) Three-Dimensional Metamaterial Lens Antennas, *Antennas and Propagation (EUCAP), Proceedings of the 5th European Conference,* pp. 3301 - 3303 , ISBN: 978-1-4577-0250-1, Rome, 11-15 April 2011.

Lin L., Wang W., Cui J., Du C., Luo X., (2008), Design of electromagnetic refractor and phase transformer using coordinate transformation theory, *Optics Express,* Vol.16, n°10, pp.6815-6821.

Huangfu J., Xi S., Kong F., Zhang J., Chen H., Wang D., Wu B.J., Ran L., Kong J.A., (2008) Application of coordinate transformation in bent waveguides, *Journal of Applied Phys*ics Vol.104, 014502.

Tichit P.H., Burokur S.N., de Lustrac A., (2010), Waveguide taper engineering using coordinate transformation technology, *Optics Express*, Vol.18, n°2, pp. 767-772.

Ghasemi R., Tichit P.H., Degiron A., Lupu A. de Lustrac A., (2010), Efficient control of a 3D optical mode using a thin sheet of transformation optical medium, *Optics Express*, Vol.18, n 19, pp. 20305-20312.

Liu R., Ji C., Mock J.J., Chin J.Y., Cui T.J., Smith D.R., (2009), Broadband Ground-Plane Cloak, *Science*, Vol.323, pp.366-369.

Xu X., Feng Y., Hao Y., Zhao J., Jiang T., (2009), Infrared carpet cloak designed with uniform silicon grating structure, *Applied Physics Letters,* Vol.95, pp 184102.

Valentine J., Li J., Zentgraf T., Bartal G., Zhang X., (2009), An optical cloak made of dielectrics, *Nature Materials*, Vol.8, pp.568-571.

Gabrielli L. H., Cardenas J., Poitras C.B., Lipson M., (2009), Silicon nanostructure cloak operating at optical frequencies, *Nature Photonics* Vol.3, pp.461-463.

Greenleaf A., Kurylev Y., Lassas M., and Uhlmann G., (2007), Electromagnetic Wormholes and Virtual Magnetic Monopoles from Metamaterials, *Physical Review Letters*, Vol.99, 183901.

Cheng, Q. & Cui, T. J. (2009), An omnidirectional electromagnetic absorber made of metamaterials, *New Journal of Physics*, Vol.12, 063006

Djermoun A., de Lustrac A., Lourtioz J.M., (2007), A wide band left handed material with high transmission, *Photonics and Nanostructures - Fundamentals and Applications*, Vol.5, n1, pp. 21-28.

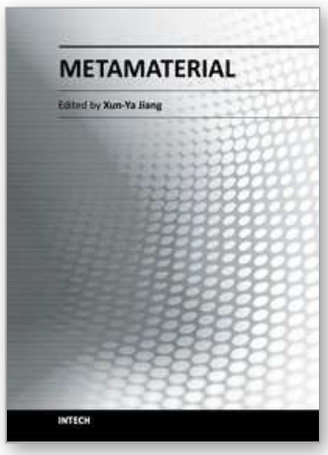

Metamaterial

Edited by Dr. Xun-Ya Jiang

ISBN 978-953-51-0591-6
Hard cover, 620 pages
Publisher InTech
Published online 16, May, 2012
Published in print edition May, 2012

In-depth analysis of the theory, properties and description of the most potential technological applications of metamaterials for the realization of novel devices such as subwavelength lenses, invisibility cloaks, dipole and reflector antennas, high frequency telecommunications, new designs of bandpass filters, absorbers and concentrators of EM waves etc. In order to create a new devices it is necessary to know the main electrodynamical characteristics of metamaterial structures on the basis of which the device is supposed to be created. The electromagnetic wave scattering surfaces built with metamaterials are primarily based on the ability of metamaterials to control the surrounded electromagnetic fields by varying their permeability and permittivity characteristics. The book covers some solutions for microwave wavelength scales as well as exploitation of nanoscale EM wavelength such as visible specter using recent advances of nanotechnology, for instance in the field of nanowires, nanopolymers, carbon nanotubes and graphene. Metamaterial is suitable for scholars from extremely large scientific domain and therefore given to engineers, scientists, graduates and other interested professionals from photonics to nanoscience and from material science to antenna engineering as a comprehensive reference on this artificial materials of tomorrow.

INTECH
open science | open minds

InTech Europe
University Campus STeP Ri
Slavka Krautzeka 83/A
51000 Rijeka, Croatia
Phone: +385 (51) 770 447
Fax: +385 (51) 686 166
www.intechopen.com

InTech China
Unit 405, Office Block, Hotel Equatorial Shanghai
No.65, Yan An Road (West), Shanghai, 200040, China
中国上海市延安西路65号上海国际贵都大饭店办公楼405单元
Phone: +86-21-62489820
Fax: +86-21-62489821

IntechOpen